HHS Public Access

Author manuscript

Brain Struct Funct. Author manuscript; available in PMC 2021 July 01.

Published in final edited form as:

Brain Struct Funct. 2020 July ; 225(6): 1743–1760. doi:10.1007/s00429-020-02090-x.

BTBD9 and dopaminergic dysfunction in the pathogenesis of Restless Legs Syndrome

Shangru Lyu[a], **Atbin Doroodchi**[c], **Hong Xing**[a], **Yi Sheng**[b], **Mark P. DeAndrade**[a], **Youfeng Yang**[c], **Tracy L. Johnson**[d], **Stefan Clemens**[d], **Fumiaki Yokoi**[a], **Michael A. Miller**[c], **Rui Xiao**[b], **Yuqing Li**[a]

[a]Norman Fixel Institute for Neurological Diseases, Department of Neurology, College of Medicine, University of Florida, Gainesville, FL, 32610, USA;

[b]Department of Aging and Geriatric Research, College of Medicine, University of Florida, Gainesville, FL, 32610, USA;

[c]Department of Cell, Developmental and Integrative Biology, the University of Alabama at Birmingham, Birmingham, AL, 35294, USA;

[d]Department of Physiology, Brody School of Medicine, East Carolina University, Greenville, NC 27834, USA.

Abstract

Restless Legs Syndrome (RLS) is characterized by an urge to move the legs, usually accompanied by uncomfortable sensations. RLS symptoms generally happen at night and can be relieved by movements. Genetic studies have linked polymorphisms in *BTBD9* to a higher risk of RLS. Knockout of *BTBD9* homolog in mice (*Btbd9*) and fly results in RLS-like phenotypes. A dysfunctional dopaminergic system is associated with RLS. However, the function of *BTBD9* in the dopaminergic system and RLS is not clear. Here, we made use of the simple *Caenorhabditis elegans* nervous system. Loss of *hpo-9*, the worm homolog of *BTBD9*, resulted in hyperactive egg-laying behavior. Analysis of genetic interactions between *hpo-9* and genes for dopamine receptors (*dop-1, dop-3*) indicated that *hpo-9* and *dop-1* worked similarly. Reporter assays of *dop-1* and *dop-3* revealed that *hpo-9* knockout led to a significant increase of DOP-3 expression. This appears to be evolutionarily conserved in mice with an increased D_2 receptor (D_2R) mRNA in the striatum of the *Btbd9* knockout mice. Furthermore, the striatal D_2R protein was significantly decreased and the dynamin I was increased. Overall, activities of DA neurons in the substantia nigra were not altered, but the peripheral D_1R pathway was potentiated in the *Btbd9* knockout mice. Finally, we generated and characterized dopamine neuron-specific *Btbd9* knockout mice and

[1]The content is solely the responsibility of the authors and does not necessarily represent the official views of the National Institutes of Health.

Corresponding author: Yuqing Li, Ph.D., Department of Neurology, College of Medicine, University of Florida, PO Box 100236, Gainesville, Florida 32610-0236; yuqing.li@neurology.ufl.edu, Phone 352-273-6546; Fax: 352-273-5989.

Conflict of interest

The authors declare that they have no conflicts of interest with the contents of this article1.

Human and animal rights

This article does not contain any studies with human participants performed by any of the authors. All procedures performed in studies involving animals were in accordance with the ethical standards of East Carolina University and the University of Florida.

detected active-phase sleepiness, suggesting that dopamine neuron-specific loss of *Btbd9* is sufficient to disturb the sleep. Our results suggest that increased activities in the D_1R pathway, decreased activities in the D_2R pathway, or both may contribute to RLS.

Keywords

restless legs syndrome; *Btbd9*; *hpo-9*; dopamine receptors; dynamin-1

Introduction

Restless legs syndrome (RLS) is a common neurological disorder characterized by a strong urge to move the legs, with or without unpleasant sensations in lower limbs, which can generally be relieved by movements (Garcia Borreguero et al., 2017). As these symptoms predominately occur in the evening or at night, the disease often leads to a disruption of sleep and a poor quality of life (Abetz et al., 2004; Trenkwalder et al., 2005). Prescription medications for RLS patients include D_2/D_3 dopaminergic agonists (Garcia-Borreguero et al., 2016; Ferre et al., 2017; Trenkwalder et al., 2018).

Several studies have suggested the involvement of the dopaminergic system in the RLS. A higher concentration of BH_4 (Earley et al., 2001, 2006), which is a rate-limiting cofactor for tyrosine hydroxylase (TH) (Meiser et al., 2013), and an increased level of 3-ortho-methyldopa (Earley et al., 2006; Allen et al., 2009), a metabolite of L-DOPA (Allen et al., 2009), have been found in the cerebrospinal fluid of RLS patients. Autopsy studies show decreased (D_2 dopamine receptor) D_2R expression in the putamen and increased phosphorylated TH in both putamen and substantia nigra (SN) (Connor et al., 2009). Brain imaging studies show decreased dopamine transporter (DAT) (Earley et al., 2011) and D_2R binding potential (Michaud et al., 2002; Earley et al., 2013), and a strong correlation between the loss of D_2R and the severity of RLS (Connor et al., 2009).

Dopamine (DA) binds to the postsynaptic DA receptors or presynaptic DA autoreceptors after released into the synaptic cleft (Meiser et al., 2013; Koblinger et al., 2014). There are two classes of DA receptors, D1-like and D2-like. The D_1 DA receptor (D_1R) is involved in the direct pathway, while D_2R participates in the indirect pathway (Keeler et al., 2014). The classic model indicates that direct pathway enables movement and is pronociceptive, while the indirect pathway inhibits movement and is antinociceptive (Ben-Sreti et al., 1983; Rooney and Sewell, 1989; Zarrindast and Moghaddampour, 1989; Verma and Kulkarni, 1993; Hore et al., 1997; Gao et al., 2000; Wall et al., 2013). Therefore, direct and indirect pathways work in a coordinated manner in motor control and nociception (Klaus et al., 2019).

Genome-wide association studies (GWAS) have implicated that up to 19 risk loci, including single nucleotide polymorphisms (SNPs) in *BTBD9* intron 5, increase the susceptibility to RLS (Stefansson et al., 2007; Winkelmann et al., 2007; Schormair et al., 2017). As a leading gene associated with RLS, *BTBD9* encodes a protein belonging to the BTB (POZ) protein family, which is ubiquitously expressed and modulates cytoskeleton arrangement, transcription repression, and protein ubiquitination (Stefansson et al., 2007; Winkelmann et

al., 2007). A loss of the *BTBD9* homolog, *Btbd9*, in mice is linked to altered hippocampal synaptic plasticity and enhanced learning and memory (DeAndrade et al., 2012b). Furthermore, both mice and fruit flies with knockouts of *BTBD9* homologs show RLS-like phenotypes. Specifically, *Btbd9* complete knockout mice develop motor restlessness, disrupted sleep, and altered sensory perception (DeAndrade et al., 2012a). The sensory deficit of knockout mice can be relieved by ropinirole, a DAergic agonist widely used for RLS treatment (DeAndrade et al., 2012a). Similarly, loss of the *BTBD9* homolog in *Drosophila melanogaster*, *CG1826*, results in increased motor activity, decreased DA levels, and disrupted sleep patterns (Freeman et al., 2012). The sleep phenotype can be reproduced by RNAi-mediated knockdown of *CG1826* in a subset of DA neurons (Freeman et al., 2012). In conclusion, these observations suggest that loss-of-function in BTBD9 can lead to abnormal DAergic function and RLS pathogenesis; however, the mechanisms through which mutations of *BTBD9* lead to DAergic dysfunction and RLS-like phenotypes are not known.

To determine if the loss of BTBD9 in DA neurons alone can cause RLS-like phenotypes in mice, we characterized the egg-laying and locomotor behaviors of a mutant *Caenorhabditis elegans* (*C. elegans*) strain, in which the *BTBD9* homolog, *hpo-9*, was knocked out. Because of the simple nervous system and the ease of making genetic crosses in worms, we were able to investigate the relationship of the *BTBD9* homolog and DA receptors. This was followed by complementary studies in *Btbd9* complete knockout mice. Furthermore, we generated DA neuron-specific *Btbd9* knockout mice (*Btbd9* dKO) using the *Cre-loxP* system and analyzed their sensorimotor behaviors related to RLS.

Materials and methods

C. elegans strains

C. elegans strains were maintained on nematode growth media (NGM) plates seeded with *Escherichia coli* strain OP50 at 20°C using standard methods unless otherwise noted. The wildtype (WT) strain used in this study was Bristol N2. The *hpo-9*(*tm3719*) strain was obtained from the National BioResource Project (Japan). The *hpo-9(tm3719)* strain lacks nucleotides 12131/12132 to 12892/12893 (761 bp deletion) of cosmid C05C8 (Figure 1A). The *hpo-9(tm3719)* mutant was backcrossed four times to the N2 background. PCR was used to genotype the *tm3719* allele (KO1: 5'-ACAAATCTGTTGTACAACATCTT-3' and KO2: 5'-GATAGTGTGGAATTATATTCGTGT-3', Figure 2A) and the wild-type (WT1: 5'-CAGCAATAAGCGAATATTTCAAGG-3' and WT2: 5-AATCTCTCGCAAGAAGCTCC-3', Figure 1A). Strains obtained from Caenorhabditis Genetics Center (University of Minnesota, Twin Cities) are *dop-1(vs100)*, *dop-3(vs106)*, *dop-1(vs100)*; *dop-3(vs106)*, and *vsIs33*; *lin-15B&lin-15A(n765)*; *vsIs28*. To generate *hpo-9(tm3719);dop-1(vs100)*, *hpo-9(tm3719);dop-3(vs106)* double knockouts, *hpo-9(tm3719)*;*dop-1(vs100)*; *dop-3(vs106)* triple knockouts, and *hpo-9(tm3719)*; *dop-1::gfp*; *dop-3::rfp* strain, we induced *hpo-9(tm3719)* mutant males by heat shock (34° C) and crossed them into *dop-1(vs100)*, *dop-3(vs106)*, *dop-1(vs100)*; *dop-3(vs106)* and *vsIs33*; *lin-15B&lin-15A(n765)*; *vsIs28* respectively using standard method. Double and triple mutants were confirmed by fluorescence and PCR (*dop-1* forward: 5'-GTGTGCTGGCTTCCGTTCTTC-3'; *dop-1* reverse: 5'-

GATTCAGGCGAGTTGCATTCG-3'; *dop-3* forward: 5'-CCAGAAAGCGTCCCATCTTCC-3'; *dop-3* reverse: 5'-GACCGCGCTGAACCAAAGTATG-3'), with target size of 291 bp for *dop-1* knockout and 384 bp for *dop-3* knockout, respectively.

Egg retention assay

The number of eggs retained *in utero* was measured as previously described (Chase and Koelle, 2004). Briefly, larval stage 4 (L4) worms (n=10–20 for all strains) were isolated and allowed to mature at 20°C for 22 hrs. Next, young adult worms were placed individually in a solution of sodium hypochlorite, which dissolves the worm but leaves the eggs intact. The number of eggs sustained was counted within 10 to 20 min, and the developmental stages of the eggs were identified and scored (Ringstad and Horvitz, 2008).

Egg-laying assay

To count the number of eggs laid in 5 days, we obtained synchronized young adult worms (n=12 for both strains) as described above. Worms were isolated and placed on individual NGM plate seeded with OP50 for 24 hrs. Subsequently, each adult worm was moved to a new plate, and the number of eggs left on the previous plate was counted. This step was repeated 5 times, and the total number of eggs laid in 5 days was counted for each worm. To identify and score developmental stages of eggs laid, we isolated and placed synchronized young adult worms (n=8–12 for both strains) on NGM plate seeded with OP50 for 1 hr. The scores were given according to others (Ringstad and Horvitz, 2008).

RNA interference

RNAi against *hpo-9* (*hpo-9* RNAi) (Kamath et al., 2003), or an empty vector (EV) was used according to a standard feeding method with HT115 bacterial strain (Kamath et al., 2001). Briefly, adult worms laid eggs on a plate covered with bacteria containing the *hpo-9* RNAi (n=8) or the EV (n=7). Then the adult worms were removed, and the progeny grew on that plate until the L4 stage. The worms were then transferred to another plate seeded with the HT115 containing the same RNAi or EV. After 22 hrs, eggs retained *in utero* were counted as described above.

DA modulation of egg retention

Synchronized young adult worms (n=11–16) were placed in 8 mM DA solution freshly dissolved in NGM buffer or NGM buffer alone for 1 hr, after which they were dissolved by sodium hypochlorite and the number of eggs unlaid was counted. The protocol was modified from (Weinshenker et al., 1995).

WormLab

Worms used for filming were all at the age of 24 hrs following L4. Movies for behavioral analyses were obtained using the WormLab system (MBF Bioscience) and were acquired at a rate of 14 frames/s at room temperature (22–24°C).

For locomotor assays on agar, an individual worm was transferred to fresh 5 cm NGM agar plates thinly seeded with OP50 and allowed to acclimate for 1–2 min before filming. In all

cases, 2 min digital video of the individual worm was captured and then analyzed using the WormLab software. All parameters were kept constant at the manufacturer's recommended settings except that the threshold was adjusted individually to maximize the optimal recognition of worms.

Imaging and fluorescence quantification

Worms were mounted on a 1% agarose pad and analyzed with a CCD camera (Qimaging optiMOS) on an Olympus BX51 microscope at 40× magnification. GFP or RFP intensity was measured in mean gray value (backgrounds were subtracted with rolling ball radius of 200 pixels) from the head region right behind the support cells and ended after the nerve ring using ImageJ (Thompson et al., 2014). The experiment was repeated twice. For the first batch, 10 *dop-1::gfp; dop-3::rfp* worm and 20 *hpo-9(tm3719); dop-1::gfp; dop-3::rfp* were used. For the second batch, 30 animals were quantitated for each strain. The representative pictures were captured at 10× magnification.

Mice

All experimental procedures complied with the National Institutes of Health guidelines for animal care and the Institutional Animal Care and Use Committees at East Carolina University and the University of Florida. *Btbd9 loxP* mice were imported from the European Mouse Mutant Archive (EMMA) (EMMA ID: 05554) in which the 4th exon of the *Btbd9* gene is flanked by *loxP* sites. Generation of the *Btbd9* complete knockout mice was performed as described (Lyu et al., 2019b). Most of the experiments were conducted with males to minimize the variations caused by estrous cycles in females.

Dat-cre mice were imported from Jackson's Lab (stock no. 6660) and used to breed with *Btbd9 loxP* mice to obtain *Dat-cre* and *Btbd9 loxP* double heterozygous mice. When *cre* and *loxP* sites are present in the offspring, *Cre*-mediated recombination occurs around the 4th exon, resulting in the loss of the 4th exon and a frameshift mutation, thereby effectively leading to the inactivation of *Btbd9* gene specifically in DA neurons (Figure 9A). Double heterozygous mice (*Dat-cre+/-Btbd9 loxP+/-*) were used for breeding with hetero- or homozygous *Btbd9 loxP* mice to generate the experimental mice in which *cre* is expressed and *loxP* sites exist in both alleles (*Dat-cre+/-Btbd9 loxP−/−*, *Btbd9* dKO) and control groups, including WT littermates, *Dat-cre+/-* mice, and animals only having *loxP* sites in one allele (*Btbd9 loxP+/-*) or both of alleles (*Btbd9 loxP−/−*). PCR was used for genotyping the *Dat-cre* (common forward: TGG CTG TTG GTG TAA AGT GG; WT reverse: GGA CAG GGA CAT GGT TGA CT; mutant reverse: CCA AAA GAC GGC AAT ATG GT) and the *loxP* sites (forward: ACA TCA CCC ATT ACT TAG AAC CTC; reverse: CAC AGC TAT TTC CTG TCA TTC TGG ACA). To confirm the specific deletion of *Btbd9* in DA neurons, we dissected out brain regions following the protocol (Spijker, 2011). PCR was used to detect null alleles with primers (forward: CAT GTG AAG TGG AGC AAA GGA; reverse: GAA CCT CTA TGT GTG CTA CCT) (Figure 9B). The mice were housed under normal 12 hrs light and 12 hrs dark condition (12 LD).

Open field

Seven naïve *Btbd9* dKO and 8 naïve male control littermates at an average age of 4 months were used in the open field analysis as previously described (Dang et al., 2005) during midday. Briefly, each mouse was placed in the center of a VersaMax Legacy open field apparatus connected to a computerized Digiscan System (Accuscan Instruments, Inc. OH) and continuously monitored for 30 min. Bright illumination (approximately 1 k lux at the center by a 60 W white bulb) was focused on the center of each field.

Continuous open field

Five naïve *Btbd9* dKO and 8 untested male control littermates were used in the experiment. The animals have an average age of 4 months and were maintained on 12 LD for 7 days. As described previously (Meneely et al., 2018; Lyu et al., 2019a; Lyu et al., 2019b; Lyu et al., 2019c), each mouse was placed in the center of a VersaMax Legacy open field apparatus with enough corncob bedding, food, and water. The apparatus contains infrared sensors along the walls that detect any breaks in the beams, which are then decoded by VERSDATA version 2.70–127E (AccuScan Instruments INC.) into behavioral patterns. The data was recorded every 15 min (15 min bin) throughout the experiment. Only the last 4 days of data were analyzed. To compare the total distance traveled between *Btbd9* dKO and WT, we separated the data into the light cycle and the dark cycle. Each cycle contains 4 periods, from day 4 to day 7, or night 4 to night 7. The distance traveled during each period was added up from the 15 min bins. To compare the probability of waking between the two groups, we recoded the data according to the total distance traveled during each 15 min bin. If the total distance traveled during the 15 min was 0, the mouse was considered as sleeping, and the data were coded as 0; otherwise, the mouse was considered as awake, and the data were coded as 1.

Wheel running

Ten *Btbd9* dKO male mice and 10 male control littermates at an average age of 4 months were maintained under a 12 LD condition for 7 days. Most of the animals had been tested in the short open field experiment except 3 dKO and 2 controls, which were naive. Wheel running activity was recorded as the number of wheel revolutions occurring during 5 min bins and analyzed using Lafayette Instrument Activity Wheel Monitor software. The activities from the 4th to the 7th day were included in the data analysis, grouped by light phase and dark phase.

Tail flick

Nine male *Btbd9* dKO mice and 12 male control littermates at an average age of 7 months were tested for the perception of warm stimuli using the Tail Flick Analgesia Meter (San Diego Instruments) as previously described (DeAndrade et al., 2011). Seven dKO and 8 control mice had been tested with short open field followed by wheel running. Two dKO and 2 control mice had been tested with wheel running only. Two additional new naive controls were used in the experiment. Briefly, each mouse was placed in an acrylic restrainer with the distal end of its tail protruding under a heat lamp. The lamp, together with a timer, was

turned on, both of which stopped automatically when the mouse flicked its tail away from the light. The latency to respond was limited to 30 s to avoid injury to the mouse.

Western blot

Western blot was performed as previously described (Yokoi et al., 2015). The striata were dissected from 7 *Btbd9* complete knockout and 6 WT with an average age of 8 months at midday, and 6 *Btbd9* complete knockout and 7 WT with an average age of 8 months at midnight. The mice did not have any behavioral testing history. The lumbar spinal cords were dissected from 5 *Btbd9* complete knockout and 3 WTs with an average age of 5 months. Tissues were homogenized in 200 μl of ice-cold lysis buffer (Tris/HCL 50mM, pH=7.4; NaCl 175 mM; EDTA 5mM, pH=8.0) containing protease inhibitor cocktail (Roche). 22 μl of ice-cold 10% Triton X100 was added in the homogenate. The mixtures were incubated for 30 min on ice and centrifuged at 10,000 × g for 15 min at 4°C. The supernatant was used as protein samples for Western blot. The protein concentration of the supernatant was measured by protein assay reagent (Bio-Rad). An aliquot of the supernatant corresponding to 30 μg of protein was mixed with 2× loading buffer containing 2-mercaptoethanol and boiled for 5 min, chilled on ice and spun down. The proteins were separated on a 10% SDS-PAGE gel and transferred to Millipore Immobilon–FL transfer membranes (PVDF). The PVDF membranes were washed in 0.1M PBS for 5 min and blocked with LI-COR Odyssey blocking buffer for 1 hr. The membranes were incubated overnight at 4°C with rabbit polyclonal D_1R antibody (Abcam, ab20066) at 1: 2000 dilution (for striata) or mouse monoclonal D_1R antibody (Abcam, ab78021) at 1: 500 dilution (for spinal cords), mouse monoclonal D_2R antibody (Santa Cruz, sc-5303) at 1:500 dilution, goat polyclonal dynamin I (Santa Cruz, sc-6402) at 1:1000 dilution or goat glyceraldehyde-3-phosphate dehydrogenase (GAPDH) antibody (Santa Cruz, sc-20357) at 1:2000 dilution in the blocking buffer. The membranes were washed with 0.1M PBS containing 0.1% Tween 20 for 4 times at 5 min each, then treated for 1 hr with LI-COR IRDye 680RD donkey anti-rabbit IgG (H+L), LI-COR IRDye 800CW donkey anti-mouse IgG (H+L), or LI-COR IRDye 800CW donkey anti-goat IgG (H+L) at 1:15,556 dilution. After being washed 4 times with 0.1M PBS containing 0.1% Tween 20 for 5 min each and 0.1M PBS 3 times for 5 min each, the membranes were dried, and the signals were detected and quantified by an LI-COR Odyssey imaging system.

Quantitative RT-PCR

To determine whether mRNA levels of D_1R and D_2R were altered, we performed quantitative PCR by using CFX real-time PCR detection system (Bio-Rad) with SYBR Select Master Mix for CFX (life technologies) and PCR primer sets as described before (Dang et al., 2012; Yokoi et al., 2015). In brief, 3 *Btbd9* complete knockout and 3 WT naïve mice at an average age of 4 months were sacrificed during midday. A separate cohort of 4 *Btbd9* complete knockout and 5 WT naïve mice at an average age of 3 months were sacrificed at midnight. Their striata were dissected out and flash-frozen in liquid nitrogen. RNA was extracted using an RNAeasy Mini kit (Qiagen) according to the manufacturer's instructions. Next, cDNA was made using SuperScript III reverse transcriptase (Invitrogen). The relative quantity of cDNA for D_1R and D_2R to that of β-actin was calculated by CFX Manager™ Software #1845000.

In Vitro recording of DA neurons in SN

The experiment was conducted with 5 *Btbd9* complete knockout and 3 WT naïve male littermates with an average age of 8 months. The electrophysiological recordings were performed by investigators blind to the genotypes. Mice were deeply anesthetized by the inhalation of isoflurane and then decapitated. The brains containing the midbrain part were rapidly removed and cut coronally into 250 μm-thick slices in ice-cold, oxygenated cutting saline (in mM: 180 sucrose, 2.5 KCl, 1.25 NaH_2PO_4, 25 $NaHCO_3$, 10 D-glucose, 2 $CaCl_2$, 10 $MgCl_2$, and 10 glucose) using a Vibratome (Leica VT 1000s). The slices were recovered in a holding chamber for 60 min at 35°C with artificial cerebrospinal fluid (ACSF). Final concentrations of ACSF (in mM): 126 NaCl, 2.5 KCl, 1.25 NaH_2PO_4, 25 $NaHCO_3$, 1 $MgCl_2$, 2 $CaCl_2$, and 10 glucose. The slices were then incubated at room temperature until use. Slices were placed in a recording chamber and continuously perfused with ACSF, which was bubbled with 95% O_2 / 5% CO_2 at 34.5–35.5°C at a rate of 1.5 ml/min and visualized with an upright microscope (Zeiss, Germany) using a 40× water-immersion objective with infrared optics. The DA neurons were identified by large cell body and triangular multipolar shape in the SN pars compacta.

Cell-attached recording electrodes were filled with a K-gluconate-based solution containing the following (in mM): 130 K-gluconate, 10 HEPES, 0.6 EGTA, 5 KCl, 4 $MgCl_2 \cdot 6H_2O$, 3 Na_2ATP, 0.3 Na_3GTP and 10 Na_2-phosphocreatine, pH 7.3 with KOH (270–280 mOsm/l) and had resistances of 5–10 MΩ. While approaching the cell, the patch electrode was applied with positive pressure. The seal (> 5 GΩ) between the recording pipette and the cell membrane was obtained by applying suction to the electrode. Action potential currents were recorded in a voltage-clamp mode, which maintained an average 0 pA holding current.

After breaking through the membrane, cell properties (capacitance, input resistance, and time constant) were obtained while the membrane potential was held at −70 mV. Resting membrane potentials were recorded in current clamp mode. Depolarizing and hyperpolarizing incremental current steps (25pA) of 1000 ms were delivered to trigger action potentials for current step recording. Then hyperpolarizing current steps of 500 ms were delivered to produce a prominent time-dependent sag in the voltage deflection; this process was repeated at 9 increasingly hyperpolarized potentials with incremental current steps (25pA).

All experiments were recorded at 32±0.5°C by a dual automatic temperature controller (TC-344B). Cell-attached recording and whole-cell recording were obtained from DA neurons using Axopatch 1D Amplifier (Molecular Devices), and data were acquired using pCLAMP 10 software (Molecular Devices, USA). Signals were filtered at 5 kHz, digitized at 10 kHz with a DigiData 1440 (Molecular Devices, Union City, CA). Cell firing activity was recorded in the form of action potential currents, which were detected by the Mini Analysis Program.

Recording of spinal reflex amplitudes (SRAs)

Experimental procedures have been described in detail previously (Clemens and Hochman, 2004; Keeler et al., 2012). Neonatal WT and *Btbd9* complete knockout mice (P7–14, WT:

n=8, *Btbd9* heterozygous knockout: n=6, *Btbd9* homozygous knockout: n=4) were anesthetized and decapitated, with the spinal cord rapidly dissected out in a Sylgard-lined Petri dish containing aerated (95% O_2 / 5% CO_2) artificial cerebrospinal fluid (ACSF) (in mM): 125 NaCl, 2.5 KCl, 2 $CaCl_2$, 1 $MgCl_2$, 25 glucose, 1.25 NaH_2PO_4, and 26 $NaHCO_3$, pH 7.4. After the opening of the dura mater, spinal cords were hemisected, and pairs of suction electrodes were attached to corresponding dorsal and ventral lumbar roots on each hemisect. After a resting phase of ~ 60 min at room temperature, reflex responses were elicited with a constant current stimulator (Iso-Stim 01D, NPI Electronics, Tamm, Germany) with pulses of 100–500 μA, 50–250 μs, at intervals of 30–60 s. Spinal reflex responses were recorded from corresponding ventral roots with a 4-channel differential AC amplifier (Model 1700, A-M Systems, Sequim, WA), digitized with a Digidata 1440A, and analyzed with the pClamp software package (Molecular Devices, Sunnyvale, CA). Reflex responses were recorded and analyzed by rectified integration. After establishing stable baseline recordings, we tested for the effects of DA D_1R agonist, SKF 38393 (Tocris, Ellisville, MO, 10 μM), on SRAs. SKF 38393 was bath-applied for durations of 30–60 min and subsequently washed out for equally long epochs. Using SigmaPlot (Systat Software, Inc., San Jose, CA), we compared SRA responses during the last 10 min of the drug perfusion protocol with those of the last 10 min in ACSF alone. All experiments were performed under “double-blind” conditions, with the experimenters at ECU unaware of the genetic makeup of the animals studied. At the end of the dissection process, tails were harvested and sent to the Li-lab for genotyping. Only after successful genotyping were the electrophysiological datasets matched to the respective WT and the 2 *Btbd9* knockout groups.

Statistical analysis

Data were tested for normality using the SPSS statistical package before analysis. The open field data and fluorescence intensity were normally distributed and analyzed by mixed model ANOVA (SAS statistical package). Data of continuous open field, tail flick, wheel running, and electrophysiological recording of DA were not normally distributed and analyzed by generalized mixed linear model (GENMOD) using a GEE model for repeated measurement (SAS), which log-transformed the data and then normalized the WT or the control group to 0 without the error bar. The age of mice was used as covariates in both ANOVA and GENMOD. For the spontaneous activity of DA, cell ID was nested within the animal ID. For the current step recording of DA, both cell ID and the intensity of currents were nested within the animal ID. The number of laid or unlaid eggs, WormLab data, qRT-PCR and the Western blot results were analyzed by Student’s *t*-test. The distribution of the stages of unlaid and laid eggs was analyzed by Wilcoxon Mann-Whitney rank-sum test, a nonparametric test.

Results

Hyperactive egg-laying behavior in *hpo-9(tm3719)* mutant *C. elegans*

Compared with mice, *C. elegans* have a much simpler nervous system and are a strong tool for studies about genetic interactions. We obtained a *C. elegans* strain with the *Btbd9* homolog gene, *hpo-9*, knocked out. We first measured the egg-laying behavior because it is known to be influenced by DA (Schafer and Kenyon, 1995; Schafer, 2005). Egg-laying

behavior is quantified by counting either the number of eggs laid or the number of eggs retained in the uterus, which is determined by the rates of egg production and egg laying. Egg-laying occurs about every 20 min (Waggoner et al., 1998), while the number of unlaid eggs or egg retention assay is a measurement of egg-laying behavior over many hours. An egg retention assay removes any variations in egg-laying rates and provides an indirect readout of egg-laying behavior that is both sensitive and consistent (Chase and Koelle, 2004; Gardner et al., 2013). The egg production rate can be quantified by the determination of brood size over the lifetime of a worm (Hodgkin and Barnes, 1991). Finally, the egg-laying deficit can also be detected by examining the developmental stages of the eggs laid and retained in the uterus (Trent et al., 1983; Ringstad and Horvitz, 2008).

hpo-9(tm3719) worms retained significantly fewer eggs *in utero* compared to N2 worms (Figure 1B, $p<0.0001$). Similarly, knocking down *hpo-9* using RNA interference (RNAi) in N2 worms resulted in a significantly reduced number of eggs *in utero* (Figure 1C, $p=0.001$), suggesting that *hpo-9*(*tm3719*) worms exhibit hyperactive egg-laying behavior. We investigated further by measuring the stages of eggs held in the uterus and those that were freshly laid. There were significantly more unlaid eggs at earlier embryonic stages in the uterus of *hpo-9(tm3719)* than N2 worms (Figure 1F). In addition, *hpo-9(tm3719)* laid significantly more eggs at early development stages compared to N2 worms (Figure 1G). These results suggest a hyperactive egg-laying behavior in the *hpo-9(tm3719)*. Finally, egg production was determined by the number of eggs produced over five days. We found that *hpo-9(tm3719)* worms had a significantly increased brood size than the N2 worms (Figure 1D, $p=0.02$).

DAergic modulation of egg-laying in *hpo-9(tm3719)* mutants

To determine if *hpo-9* knockout can cause an altered response to exogenous DA, we applied the drug and quantified the egg retention and locomotion behaviors with *hpo-9(tm3719)* and N2 worms. Synchronized adult worms were placed in either NGM solution or DA dissolved in NGM (8mM), and the egg retention assay was conducted after 1 hour. Application of DA significantly increased the number of eggs retained in both N2 and *hpo-9(tm3719)* worms (Figure 2, N2, $p=0.003$, *hpo-9 (tm3719)*, $p=0.04$), which is consistent with previous findings that DA and DAergic receptor agonists could inhibit egg-laying behavior in *C. elegans* (Schafer and Kenyon, 1995). The *hpo-9(tm3719)* worms held significantly fewer eggs than N2 worms either with or without DA (Figure 2, without DA, $p<0.0001$, with DA, $p=0.0007$). The results suggest that the DA is insufficient to normalize the egg retention deficit observed in *hpo-9(tm3719)* mutants and the inhibitory effect of DA on egg-laying is intact in the *hpo-9(tm3719)* worms.

The relationship between *hpo-9*, *dop-1*, and *dop-3*

We then investigated the genetic interactions among *hpo-9* and genes for DAergic receptors. To date, four DA receptors have been identified in *C. elegans*, including D_1-like DA receptor DOP-1 and D_2-like DA receptor DOP-3 (Chase and Koelle, 2007). The functions of these DA receptors in egg-laying behavior have not been previously reported. Therefore, we performed an egg retention assay to determine whether the *dop-1* or *dop-3* mutation could impact the egg-laying behavior by egg retention assay. We found that *dop-1(vs100)* mutants

retained a similar number of eggs as N2 animals (Figure 3A, p=0.07), while *dop-3(vs106)* mutants retained significantly more eggs (Figure 3A, p=0.003). This suggests that *dop-3*, but not *dop-1*, is directly involved in the egg-laying behavior. Next, we found that knocking out *dop-1* in *dop-3(vs106)* worms decreased the number of unlaid eggs to the N2 level (Figure 3A, p=0.02), indicating that *dop-1* antagonizes with *dop-3* in the regulation of the egg-laying behavior. Moreover, application of DA did not change the numbers of unlaid eggs in both *dop-1(vs100)* and *dop-3(vs106)* (Figure 3A, *dop-1(vs100)*, p=0.94, *dop-3(vs106)*, p=0.54), which suggests that the inhibitory effect of DA on egg-laying behavior depends on both DOP-1 and DOP-3.

Next, we included *hpo-9(tm3719)* and double knockouts in the assay and observed that *hpo-9(tm3719);dop-1(vs100)* worms retained significantly more eggs than *hpo-9(tm3719)* mutants (Figure 3B, p<0.0001) but fewer eggs than *dop-1(vs100)* mutants (Figure 3B, p<0.0001) or N2 worms (Figure 3B, p=0.006). Therefore, the *dop-1* mutation partially rescues the egg retention deficit caused by the loss of HPO-9. In contrast, *hpo-9(tm3719);dop-3(vs106)* worms had the same number of eggs *in utero* as N2 worms (Figure 3B, p=0.48), more eggs than *hpo-9(tm3719)* mutants (Figure 3B, p<0.0001), but fewer eggs than *dop-3(vs106)* worms (Figure 3B, p=0.04). These results demonstrate that *dop-3* and *hpo-9* have opposing effects on the number of eggs retained and counteract each other. Thus, the *dop-3* mutation completely suppresses the hyperactive egg-laying behavior of *hpo-9(tm3719)*.

Finally, we used a locomotor study to explore the relationship between *hpo-9*, *dop-1*, and *dop-3*. It has been previously shown that *dop-3* knockout increases resistance to DA-induced paralysis and *dop-1* knockout reverses the defects resulting from the lack of DOP-3 (Chase et al., 2004). We recorded the movement speed of different strains with WormLab and found that *dop-3(vs106)* worms moved significantly faster than N2 worms (Figure 3C, p=0.002) while *hpo-9(tm3719)* or *dop-1(vs100)* mutants moved at a speed equivalent to N2 worms (Figure 3C, *hpo-9(tm3719)*, p=0.68, *dop-1(vs100)*, p=0.53). Therefore *dop-3*, but not *dop-1* or *hpo-9*, affects the worm movement speed. Knocking out *hpo-9* in either *dop-1* (Figure 3C, p=0.04) or *dop-3* single mutant worms significantly reduced the movement speed (Figure 3C, p=0.02), indicating that *dop-1(vs100)* and *dop-3(vs106)* worms, in which the DAergic systems have been disturbed, are super sensitive to the additional *hpo-9* mutation. Knocking out *dop-1* or *hpo-9* in *dop-3* knockout background reduced the movement speed of mutant worms to the N2 level (Figure 3C), suggesting that both *dop-1* and *hpo-9* antagonize with *dop-3*. Moreover, in the *dop-1(vs100); dop-3(vs106)* worms, the *hpo-9* mutation led to a significant increase in the movement speed (Figure 3C, p=0.002). In *hpo-9(tm3719); dop-3(vs106)* worms, the *dop-1* mutation also stimulated movement speed instead of being inhibitory, as in the *dop-3* single mutants (Figure 3C, p=0.007). These results suggest a functional similarity between HPO-9 and DOP-1. Finally, the effect of the *hpo-9* mutation on movement speed is highly genetic background specific. The *hpo-9* mutation did not affect the WT background, reduced movement speed in either the *dop-1* or *dop-3* single mutant background, and interestingly, significantly increased movement speed in the *dop-1* and *dop-3* double mutant background.

HPO-9 deficiency led to increased transcription of DOP-3

With two *C. elegans* behavioral assays indicating that *hpo-9* interacts with both *dop-1* and *dop-3*, we further tested the influence of *hpo-9* knockout on expression levels of these DA receptors. We crossed *hpo-9(tm3719)* with strains harboring *gfp* under the control of *dop-1* promoter and *rfp* under the control of the *dop-3* promoter. Consistent with other literature (Chase et al., 2004; Ezak and Ferkey, 2010), *dop-1* and *dop-3* expressed throughout the body, including neurons of the head, the ventral cord and the tail (Figure 4A, left panel). Expression patterns of *dop-1* and *dop-3* in the *hpo-9* mutant were similar to N2 (Figure 4A, right panel). We quantified the fluorescent intensity in the head region (Figure 4B) and found that the *hpo-9* mutation led to a significantly higher fluorescent intensity of RFP (DOP-3) (Figure 4D, p=0.02), but not GFP (DOP-1) (Figure 4C, p=0.17). The result suggests that *hpo-9* influences the transcription of DOP-3.

BTBD9 deficiency led to increased transcription of D_2R during midnight

Similarly, we tested the D_1R and D_2R mRNA levels in the striatum of *Btbd9* complete knockout mice and their WT littermates. Symptoms of RLS patients usually occur or become worse in the evening or at night (Garcia Borreguero et al., 2017). Therefore, RLS is a disease with a circadian component. We collected the mouse samples two times a day, which were midday and midnight, respectively. It should be noticed that mice have opposite day-night rhythms to humans. They usually are active during the night but are sleeping during the day. We found a similar increase of D_2R mRNA expression (Figure 5B, p=0.03; C, p=0.04), but not D_1R (Figure 5A, p=0.75), in the striatum of *Btbd9* complete knockout mice sacrificed during midnight. However, there were no significant differences in D_1 and D_2 mRNA expression during midday between WT and *Btbd9* complete knockout mice (Figure 5A, p=0.41; 5B, p=0.55; 5C, p=0.27), indicating that the influence of *Btbd9* complete knockout on mRNA level of D_2R is circadian-dependent. Interestingly, the mRNA levels of DA receptors were decreased in WT mice during the night or active phase (Figure 5A, p=0.02; 5B, p=0.04; 5C, p=0.02), but not in knockout mice (Figure 5A, p=0.12; 5B, p=0.44; 5C, p=1.00). These results suggest that BTBD9 and its homolog strongly influence the transcription of DA receptors in both worms and mice, with the later have additional circadian rhythm-dependent controls.

BTBD9 deficiency caused decreased protein level of D_2R during midday

The half-life of mRNA is generally short, and the mRNA level is not always consistent with the actual protein levels (Greenbaum et al., 2003). Therefore, we did a Western blot with mouse striatum to determine the D_1R and D_2R protein levels. D_1R protein was not altered (Figure 6A, p=0.83; Figure 6D, p=0.95), which is consistent with the RT-PCR data. Surprisingly, the D_2R protein level was significantly decreased during midday (Figure 6B, p=0.01). At midnight, the D_2R protein level showed a trend of decrease (Figure 6E, p=0.23). The result indicates that the BTBD9 mutation affects not only the D_2R mRNA level but also the D_2R protein level. The changes in the D_2R protein level may cause incoordination between D_1-mediated and D_2-mediated DAergic pathways, leading to RLS-like phenotypes.

BTBD9 deficiency caused increased protein level of dynamin 1 in mouse striatum

The internalization of D_2R is under the regulation of dynamin I (DNM-1) (Iwata et al., 1999). The previous study found an increased level of DNM-1 in the hippocampus of *Btbd9* complete knockout mice (DeAndrade et al., 2012b). Here, we determined the DNM-1 level in the striatum. There was no change in the level of the protein between *Btbd9* complete knockout and WT mice euthanized during midday (Figure 6C, p=0.33). However, the level of DNM-1 was higher in the *Btbd9* complete knockout compared with the WT euthanized at midnight (Figure 6F, p=0.01). The decreased level of D_2R may be caused by an elevated level of DNM-1.

BTBD9 deficiency did not influence the activity of DA neurons in mouse

To determine if the presynaptic part of the striatal DAergic system has altered by BTBD9 deficiency, we did an electrophysiological study with DA neurons in SN, which fire spontaneously *in vitro* in a single-spike, pacemaker pattern without bursts (Paladini et al., 2003), and are involved in motor control and reward-based learning (Berretta et al., 2010). Using patch-clamp recording in brain slices, we found that neither spontaneous firing frequency (Figure 7B, left panel, p=0.74) nor regularity (Figure 7B, right panel, p=0.27) of DA neurons was altered by the lack of BTBD9. In addition, the responses to external stimuli of DA neurons were also the same between *Btbd9* complete knockout and their WT littermates (Figure 7E, p=0.60). The result indicates that the activity of DA neurons in SN is not altered.

The response of a D_1R agonist on SRAs was diminished with BTBD9 deficiency

Both central and peripheral DAergic systems have been shown to play a role in RLS (Yokota et al., 1991; Bara-Jimenez et al., 2000; Tings et al., 2003; Bachmann et al., 2010; Marconi et al., 2012; Ferri et al., 2015). Lesions of the hypothalamic descending A11 DAergic system leads to RLS-like phenotypes (Qu et al., 2007). To test the influence of loss of BTBD9 in the spinal DAergic system, we bath-applied the SKF 38393 to the isolated spinal cords and recorded the SRAs of WT and *Btbd9* complete knockout mice. Application of SKF 38393 significantly increased SRAs of the WT mice (Figure 8A, p=0.03) as we reported earlier (Keeler et al., 2012). This stimulative function of SKF 38393, however, was absent in both the *Btbd9* heterozygous (Figure 8A, p=0.45) and homozygous knockout mice (Figure 8A, p=0.93), indicating a potentiated D_1R-mediated DAergic pathway. To test if the increased activity in D_1R-mediated DAergic pathway is caused by expression change of DA receptors, we did Western blot and found that both D_1R and D_2R protein levels in the lumbar spinal cord remained the same in *Btbd9* complete knockout mice (Figure 8B, left panel, p= 0.99; right panel, p=0.85).

No motor restlessness and thermal sensory alteration in *Btbd9* dKO mice

To determine if BTBD9 deficiency specifically in the DA neurons is enough for mice to develop RLS-like phenotypes, we generated *Btbd9* dKO mice as shown in Figure 9A (see Method). To confirm the tissue specificity of the *cre*-mediated recombination, we dissected and analyzed different parts of the brains. Only the midbrain showed the band with the right

size for the recombination, indicating *Btbd9* deletion was restricted to the midbrain DAergic neurons (Figure 9B).

The principal feature of RLS is the urge to move (Garcia Borreguero et al., 2017). Previous phenotypic mouse or fruit fly models of RLS have shown increased activity levels (Ondo et al., 2000; Clemens and Hochman, 2004; Esteves et al., 2004; DeAndrade et al., 2012a; Freeman et al., 2012). Therefore, to assess the total activity levels of the *Btbd9* dKO mice, we did both short- and long-term open field experiments. In the 30-min open field test, *Btbd9* dKO mice exhibited no change in total distance traveled (Figure 9C, left panel, p=0.75), as well as clockwise and counterclockwise circling compared with the control group (Figure 9C, right panel, CW, p=0.66, CCW, p=0.78). The continuous open field experiment did not detect any difference in total distance traveled between mutant and control mice either in the light phase (Figure 9E, light, p=0.07), when the animals are usually sleeping or resting, or during the dark phase, when the animals are active (Figure 9E, dark, p=0.67). However, *Btbd9* dKO mice showed a decreased probability of waking in the dark phase (Figure 9F, light, p=0.04), which could suggest that the mutant mice showed sleepiness during the active phase. The abnormality in the active phase suggests a decreased sleep quality in the rest phase. This result is consistent with the symptoms of RLS patients that usually begin or worsen during the rest phase and therefore, these patients usually have disrupted sleep at night and show day-time fatigue (Garcia Borreguero et al., 2017). Next, we measured the voluntary activity of these mice using a wheel running setup. *Btbd9* dKO mice showed unchanged levels of activity during both the light phase and dark phase (Figure 9D, light, p=0.33, dark, p=0.22). These data, taken together, suggest that *Btbd9* dKO mice did not exhibit alteration in motor activity but have active phase sleepiness.

RLS patients have uncomfortable sensations in legs that are usually associated with the urge to move (Garcia Borreguero et al., 2017). In our previous study, *Btbd9* complete knockout mice exhibited a sensory deficit (DeAndrade et al., 2012a) in the tail-flick test, so we tested the sensory system of *Btbd9* dKO mice with the same method (DeAndrade et al., 2012a). The mutant mice had the same level of response to the heat stimuli as the control group (Figure 9G, p=0.72), indicating that the *Btbd9* dKO mice did not exhibit altered thermal sensation. Therefore, except for the active-phase sleepiness, the *Btbd9* dKO did not have RLS-like behaviors as observed in other *BTBD9* homolog mutant animal models (DeAndrade et al., 2012a; Freeman et al., 2012).

Discussion

DA has been extensively implicated in RLS, and DA agonists targeting D_2 and D_3 receptors have been used to treat RLS patients. In this study, we employed two model systems to study the role of BTBD9 in the DAergic system and RLS. With *C. elegans*, we found HPO-9 and DOP-1 functioned similarly in both egg-laying and locomotor behaviors. HPO-9 deficiency led to increased transcription of *dop-3*. Similarly, *Btbd9* complete knockout mice had a midnight-specific elevation of striatal D_2R mRNA, but not D_1R mRNA, compared with their WT littermates. The protein level of D_2R was reduced, which may be caused by an increased level of DNM-1. Presynaptic DA activities did not change in the *Btbd9* complete knockout mice. The weakened D_2R-mediated central DAergic pathway was accompanied by

the enhanced D_1R-mediated peripheral DAergic pathway. Furthermore, knocking out BTBD9 specifically in DA neurons led to active-phase sleepiness, indicating that the loss of *Btbd9* only in DA neurons was enough to induce a sleep deficit.

Our results contribute to the understanding of the DA signaling in the egg-laying behavior of *C.elegans*. Increased number of unlaid eggs in *dop-3* but not *dop-1* mutants suggests that *dop-3*, but not *dop-1*, directly regulates egg-laying behavior. Additionally, both *dop-1* knockout and *dop-3* knockout worms showed no response to exogenous DA. Thus, DA acted through both DOP-1 and DOP-3 to regulate egg-laying behavior. Moreover, knocking out *dop-1* recovered the number of unlaid eggs of *dop-3(vs106)* to the N2 level, indicating that *dop-1* counteracted with *dop-3* in the regulation of the egg-laying behavior.

Btbd9 homolog gene, *hpo-9*, worked similarly with *dop-1*. First, both *hpo-9* knockout and *dop-1* knockout reduced egg retention in *dop-3(vs106)*. Second, the WormLab locomotion data implied that the *dop-1* or *hpo-9* mutation alone did not induce changes in locomotion. However, the *dop-1* or *hpo-9* mutation in *dop-3(vs106)* reduced the higher moving speed observed in *dop-3* single mutant worms to the N2 level, which is consistent with the antagonistic function of *dop-1* over *dop-3* found previously (Chase et al., 2004). Finally, in the *hpo-9* and *dop-3* double knockout worms, the *dop-1* mutation increased the movement speed, which was opposite from its function in *dop-3* single knockout worms. In the *dop-1* and *dop-3* double knockout worms, the HPO-9 deficiency increased the movement speed as well.

BTBD9 and its homolog participated in the transcriptional regulation of D_2 or D_2-like DA receptors. Worm reporter gene assays demonstrated an increase in *dop-3* transcription with the *hpo-9* knockout. In mice, D_2R mRNA was increased in the striatum of *Btbd9* complete knockout at least at midnight, which suggests that the influence of BTBD9 deficiency on the D_2R mRNA level is under the control of circadian rhythm. DAergic system of rodents, at least the extracellular level of DA, is under the control of circadian rhythm (Khaldy et al., 2002; Castaneda et al., 2004; Akhisaroglu et al., 2005). Here, we found that in the WT mice, D_1R, D_2L, and D_2S mRNA levels were all decreased during the active phase compared with the rest phase. This transcriptional reduction of DA receptors in the active phase was absent in the *Btbd9* complete knockout mice, which may be the reason for higher levels of mRNAs at night in the knockout mice. *Btbd9* complete knockout mice showed sleep disturbance (DeAndrade et al., 2012a), and symptoms of RLS in patients are known to be more common at night (Garcia Borreguero et al., 2017). The disruption of circadian oscillations in the transcription of DA receptor mRNAs may contribute to these results.

The D_2R protein level was decreased and significantly reduced at midday in the *Btbd9* complete knockout mice, during the peak of the sleep cycle. Regulation of mRNA translation, post-translational modifications, protein stability, and protein recycling combined dictate the final protein level in the cell. After binding with DA, D_1R and D_2R, which belong to G-protein coupled receptors (GPCRs), are transferred to intracellular compartments from the plasma membrane, a process known as internalization (Koenig and Edwardson, 1997). The internalization of D_2R is modulated by DNM-1 (Iwata et al., 1999), which showed a significant increase in the *Btbd9* complete knockout mice. It is possible that

an increased level of DNM-1 in the active phase accelerated the endocytosis of D_2R, which is usually followed by the degradation in the lysosome (Thompson et al., 2010), and caused the observed D_2R reduction in the rest phase (Figure 10). Combined with the mRNA data, the loss of transcriptional reduction of DA receptors during the active phase in *Btbd9* complete knockout may be a compensatory result in response to a decreased level of D_2R protein level (Figure 10). It is also possible that BTBD9 protein, which contains a BTB domain, participates directly in the regulation of transcription (Stogios and Prive, 2004; Stogios et al., 2005).

We found that knocking out *Btbd9* led to reduced activity in the D_2R-mediated indirect pathway in the striatum and increased activity of D_1R-mediated responses in the spinal cord. In the striatum of *Btbd9* complete knockout mice, there was a significant decrease in D_2R but not D_1R. In addition, short term corticostriatal synaptic plasticity onto the D1 medium spiny neurons (MSNs) was increased (Lyu et al., 2019c). It has been reported that RLS patients show decreased D_2R binding potential in the striatum (Michaud et al., 2002). Both the symptoms of RLS patients and the thermal sensory deficit of *Btbd9* complete knockout mice can be relieved by D_2/D_3 agonists (DeAndrade et al., 2012a). Therefore, our results are consistent with previous clinical and animal studies and help to explain the effectiveness of D_2/D_3 agonists in RLS. In addition, we also found that the isolated spinal cord of *Btbd9* complete knockout mice lost the response to SKF 38393, a D_1R agonist. The result indicates that, with BTBD9 deficiency, the activity of the D_1R-mediated DAergic system may have reached an apex so that it cannot be increased anymore. Previously, D_3-receptor knockout mice (D3KO) and iron deprived (ID) mice have been used as models for RLS (Erikson et al., 2001; Clemens and Hochman, 2004; Zhao et al., 2007). In both D3KO and ID mice, there is a significant increase of the D_1R protein expression in the lumbar spinal cord (Zhao et al., 2007; Brewer et al., 2014). In contrast, *Btbd9* complete knockout mice did not show the alteration in the D_1R protein level in the lumbar spinal cord, suggesting that the functional increase in the peripheral D_1R-mediated DAergic system in *Btbd9* complete knockout mice is not caused by protein level change. The basal ganglia output modulates the spinal cord through feedback to the cortex. Moreover, a microcircuit has been suggested to exist between the corticostriatal tract and the corticospinal tract, starting in the striatum and ending in the spinal cord (Kiritani et al., 2012). This supports the existence of a weakened D_2R-mediated pathway but an enhanced D_1R-mediated pathway in RLS. We speculate that mutations of BTBD9 might result in incoordination between the two DAergic pathways, which should normally work in regulated harmony controlling motor and sensory outputs.

Btbd9 dKO mice did not have RLS-like phenotypes, as observed in *Btbd9* complete knockout mice (DeAndrade et al., 2012a). Previously, we have found that the striatal MSN-specific *Btbd9* knockout mice exhibit significantly increased total distance traveled in 30-min open field test, increased probability of waking during the light phase but not the dark phase in the continuous open field test, elevated level of activity during the light phase but not the dark phase in the wheel running test, and increased sensitivity to the heat stimuli in the tail-flick test (Lyu et al., 2019b). On the other hand, mice with *Btbd9* specifically knocked out in cholinergic interneurons (ChI) do not show any difference in total distance traveled in 30-min open field test, and have a decreased probability of waking during the light phase but increased probability of waking during the dark phase in the continuous open

field test (Lyu et al., 2019b). Therefore, we concluded that the loss of BTBD9 protein only in MSNs, but not ChIs, can cause RLS-like phenotypes in mice. In parallel, we also knocked out *Btbd9*, specifically in the cerebral cortex. The conditional knockout mice show a significant increase in their activity level and the probability of waking during the light phase, but not during the dark phase, in the continuous open field test. The mutant mice also show decreased sensitivity to the heat stimuli in the tail-flick test (Lyu et al., 2019c). The results indicate that the cerebral cortex also participates in the generation of RLS-like phenotypes. Overall, the data suggest that striatal MSNs and the cerebral cortex, but not DA neurons, play central roles in the pathogenesis of RLS.

In summary, *hpo-9* resembled *dop-1* functionally and participated in the regulation of DOP-3 expression. BTBD9 was involved in the regulation of both mRNA and protein levels of D_2R. Loss of BTBD9 and its homolog, HPO-9, caused altered DA-regulated outputs, which may be the underlying mechanism for RLS.

Acknowledgments

We would like to thank Dr. Shohei Mitani for the *hpo-9* strain, Dr. Lin Zhang, Chad C. Cheetham, Sung Min Han, Jack Vibbert, Pauline Cottee, Jessica Winek, and Hieu Hoang for their technical assistance and stimulating discussions. This work was supported by a grant from Restless Legs Syndrome Foundation, and startup funds from the Departments of Neurology at UAB and UF, and the National Institutes of Health [grants NS54246, NS57098, NS65273, NS72872, NS74423, and NS82244]. The content is solely the responsibility of the authors and does not necessarily represent the official views of the National Institutes of Health.

References:

Abetz L, Allen R, Follet A, Washburn T, Earley C, Kirsch J, Knight H (2004) Evaluating the quality of life of patients with restless legs syndrome. Clinical therapeutics 26:925–935. [PubMed: 15262463]

Akhisaroglu M, Kurtuncu M, Manev H, Uz T (2005) Diurnal rhythms in quinpirole-induced locomotor behaviors and striatal D2/D3 receptor levels in mice. Pharmacol Biochem Behav 80:371–377. [PubMed: 15740778]

Allen RP, Connor JR, Hyland K, Earley CJ (2009) Abnormally increased CSF 3-Ortho-methyldopa (3-OMD) in untreated restless legs syndrome (RLS) patients indicates more severe disease and possibly abnormally increased dopamine synthesis. Sleep Med 10:123–128. [PubMed: 18226951]

Bachmann CG, Rolke R, Scheidt U, Stadelmann C, Sommer M, Pavlakovic G, Happe S, Treede RD, Paulus W (2010) Thermal hypoaesthesia differentiates secondary restless legs syndrome associated with small fibre neuropathy from primary restless legs syndrome. Brain 133:762–770. [PubMed: 20194142]

Bara-Jimenez W, Aksu M, Graham B, Sato S, Hallett M (2000) Periodic limb movements in sleep: state-dependent excitability of the spinal flexor reflex. Neurology 54:1609–1616. [PubMed: 10762502]

Ben-Sreti MM, Gonzalez JP, Sewell RD (1983) Differential effects of SKF 38393 and LY 141865 on nociception and morphine analgesia. Life Sci 33 Suppl 1:665–668.

Berretta N, Bernardi G, Mercuri NB (2010) Firing properties and functional connectivity of substantia nigra pars compacta neurones recorded with a multi-electrode array in vitro. J Physiol 588:1719–1735. [PubMed: 20351050]

Brewer KL, Baran CA, Whitfield BR, Jensen AM, Clemens S (2014) Dopamine D3 receptor dysfunction prevents anti-nociceptive effects of morphine in the spinal cord. Front Neural Circuits 8:62. [PubMed: 24966815]

Castaneda TR, de Prado BM, Prieto D, Mora F (2004) Circadian rhythms of dopamine, glutamate and GABA in the striatum and nucleus accumbens of the awake rat: modulation by light. J Pineal Res 36:177–185. [PubMed: 15009508]

Chase DL, Koelle MR (2004) Genetic analysis of RGS protein function in Caenorhabditis elegans. Methods in enzymology 389:305–320. [PubMed: 15313573]

Chase DL, Koelle MR (2007) Biogenic amine neurotransmitters in C. elegans. WormBook:1–15.

Chase DL, Pepper JS, Koelle MR (2004) Mechanism of extrasynaptic dopamine signaling in Caenorhabditis elegans. Nat Neurosci 7:1096–1103. [PubMed: 15378064]

Clemens S, Hochman S (2004) Conversion of the modulatory actions of dopamine on spinal reflexes from depression to facilitation in D3 receptor knock-out mice. J Neurosci 24:11337–11345. [PubMed: 15601940]

Connor JR, Wang XS, Allen RP, Beard JL, Wiesinger JA, Felt BT, Earley CJ (2009) Altered dopaminergic profile in the putamen and substantia nigra in restless leg syndrome. Brain 132:2403–2412. [PubMed: 19467991]

Dang MT, Yokoi F, McNaught KS, Jengelley TA, Jackson T, Li J, Li Y (2005) Generation and characterization of Dyt1 DeltaGAG knock-in mouse as a model for early-onset dystonia. Exp Neurol 196:452–463. [PubMed: 16242683]

Dang MT, Yokoi F, Cheetham CC, Lu J, Vo V, Lovinger DM, Li Y (2012) An anticholinergic reverses motor control and corticostriatal LTD deficits in Dyt1 DeltaGAG knock-in mice. Behav Brain Res 226:465–472. [PubMed: 21995941]

DeAndrade MP, Yokoi F, van Groen T, Lingrel JB, Li Y (2011) Characterization of Atp1a3 mutant mice as a model of rapid-onset dystonia with parkinsonism. Behav Brain Res 216:659–665. [PubMed: 20850480]

DeAndrade MP, Johnson RL Jr., Unger EL, Zhang L, van Groen T, Gamble KL, Li Y (2012a) Motor restlessness, sleep disturbances, thermal sensory alterations and elevated serum iron levels in Btbd9 mutant mice. Hum Mol Genet 21:3984–3992. [PubMed: 22678064]

DeAndrade MP, Zhang L, Doroodchi A, Yokoi F, Cheetham CC, Chen HX, Roper SN, Sweatt JD, Li Y (2012b) Enhanced hippocampal long-term potentiation and fear memory in Btbd9 mutant mice. PLoS One 7:e35518. [PubMed: 22536397]

Earley CJ, Hyland K, Allen RP (2001) CSF dopamine, serotonin, and biopterin metabolites in patients with restless legs syndrome. Mov Disord 16:144–149. [PubMed: 11215576]

Earley CJ, Hyland K, Allen RP (2006) Circadian changes in CSF dopaminergic measures in restless legs syndrome. Sleep Med 7:263–268. [PubMed: 16564215]

Earley CJ, Kuwabara H, Wong DF, Gamaldo C, Salas R, Brasic J, Ravert HT, Dannals RF, Allen RP (2011) The dopamine transporter is decreased in the striatum of subjects with restless legs syndrome. Sleep 34:341–347. [PubMed: 21358851]

Earley CJ, Kuwabara H, Wong DF, Gamaldo C, Salas RE, Brasic JR, Ravert HT, Dannals RF, Allen RP (2013) Increased synaptic dopamine in the putamen in restless legs syndrome. Sleep 36:51–57. [PubMed: 23288971]

Erikson KM, Jones BC, Hess EJ, Zhang Q, Beard JL (2001) Iron deficiency decreases dopamine D1 and D2 receptors in rat brain. Pharmacol Biochem Behav 69:409–418. [PubMed: 11509198]

Esteves AM, de Mello MT, Lancellotti CL, Natal CL, Tufik S (2004) Occurrence of limb movement during sleep in rats with spinal cord injury. Brain Res 1017:32–38. [PubMed: 15261096]

Ezak MJ, Ferkey DM (2010) The C. elegans D2-like dopamine receptor DOP-3 decreases behavioral sensitivity to the olfactory stimulus 1-octanol. PLoS One 5:e9487. [PubMed: 20209143]

Ferre S, Quiroz C, Guitart X, Rea W, Seyedian A, Moreno E, Casado-Anguera V, Diaz-Rios M, Casado V, Clemens S, Allen RP, Earley CJ, Garcia-Borreguero D (2017) Pivotal Role of Adenosine Neurotransmission in Restless Legs Syndrome. Front Neurosci 11:722. [PubMed: 29358902]

Ferri R, Proserpio P, Rundo F, Lanza A, Sambusida K, Redaelli T, De Carli F, Nobili L (2015) Neurophysiological correlates of sleep leg movements in acute spinal cord injury. Clin Neurophysiol 126:333–338. [PubMed: 24947594]

Freeman A, Pranski E, Miller RD, Radmard S, Bernhard D, Jinnah HA, Betarbet R, Rye DB, Sanyal S (2012) Sleep fragmentation and motor restlessness in a Drosophila model of Restless Legs Syndrome. Current biology : CB 22:1142–1148. [PubMed: 22658601]

Gao X, Zhang Y, Wu G (2000) Effects of dopaminergic agents on carrageenan hyperalgesia in rats. Eur J Pharmacol 406:53–58. [PubMed: 11011033]

Garcia Borreguero D, Winkelmann J, Allen RP (2017) Introduction: Towards a better understanding of the science of RLS/WED. Sleep Med 31:1–2. [PubMed: 27894926]

Garcia-Borreguero D, Silber MH, Winkelman JW, Hogl B, Bainbridge J, Buchfuhrer M, Hadjigeorgiou G, Inoue Y, Manconi M, Oertel W, Ondo W, Winkelmann J, Allen RP (2016) Guidelines for the first-line treatment of restless legs syndrome/Willis-Ekbom disease, prevention and treatment of dopaminergic augmentation: a combined task force of the IRLSSG, EURLSSG, and the RLS-foundation. Sleep Med 21:1–11. [PubMed: 27448465]

Gardner M, Rosell M, Myers EM (2013) Measuring the effects of bacteria on C. elegans behavior using an egg retention assay. J Vis Exp:e51203. [PubMed: 24192811]

Greenbaum D, Colangelo C, Williams K, Gerstein M (2003) Comparing protein abundance and mRNA expression levels on a genomic scale. Genome Biol 4:117. [PubMed: 12952525]

Hodgkin J, Barnes TM (1991) More is not better: brood size and population growth in a self-fertilizing nematode. Proc Biol Sci 246:19–24. [PubMed: 1684664]

Hore SK, Dumka VK, Kumar D, Tripathi HC, Tandan SK (1997) Central noradrenergic & dopaminergic modulation of brewer's yeast-induced inflammation & nociception in rats. Indian J Med Res 105:93–97. [PubMed: 9055502]

Iwata K, Ito K, Fukuzaki A, Inaki K, Haga T (1999) Dynamin and rab5 regulate GRK2-dependent internalization of dopamine D2 receptors. Eur J Biochem 263:596–602. [PubMed: 10406971]

Kamath RS, Martinez-Campos M, Zipperlen P, Fraser AG, Ahringer J (2001) Effectiveness of specific RNA-mediated interference through ingested double-stranded RNA in Caenorhabditis elegans. Genome Biol 2:Research0002.

Kamath RS, Fraser AG, Dong Y, Poulin G, Durbin R, Gotta M, Kanapin A, Le Bot N, Moreno S, Sohrmann M, Welchman DP, Zipperlen P, Ahringer J (2003) Systematic functional analysis of the Caenorhabditis elegans genome using RNAi. Nature 421:231–237. [PubMed: 12529635]

Keeler BE, Baran CA, Brewer KL, Clemens S (2012) Increased excitability of spinal pain reflexes and altered frequency-dependent modulation in the dopamine D3-receptor knockout mouse. Exp Neurol 238:273–283. [PubMed: 22995602]

Keeler JF, Pretsell DO, Robbins TW (2014) Functional implications of dopamine D1 vs. D2 receptors: A 'prepare and select' model of the striatal direct vs. indirect pathways. Neuroscience 282:156–175. [PubMed: 25062777]

Khaldy H, Leon J, Escames G, Bikjdaouene L, Garcia JJ, Acuna-Castroviejo D (2002) Circadian rhythms of dopamine and dihydroxyphenyl acetic acid in the mouse striatum: effects of pinealectomy and of melatonin treatment. Neuroendocrinology 75:201–208. [PubMed: 11914592]

Kiritani T, Wickersham IR, Seung HS, Shepherd GM (2012) Hierarchical connectivity and connection-specific dynamics in the corticospinal-corticostriatal microcircuit in mouse motor cortex. J Neurosci 32:4992–5001. [PubMed: 22492054]

Klaus A, Alves da Silva J, Costa RM (2019) What, If, and When to Move: Basal Ganglia Circuits and Self-Paced Action Initiation. Annu Rev Neurosci 42:459–483. [PubMed: 31018098]

Koblinger K, Fuzesi T, Ejdrygiewicz J, Krajacic A, Bains JS, Whelan PJ (2014) Characterization of A11 neurons projecting to the spinal cord of mice. PLoS One 9:e109636. [PubMed: 25343491]

Koenig JA, Edwardson JM (1997) Endocytosis and recycling of G protein-coupled receptors. Trends Pharmacol Sci 18:276–287. [PubMed: 9277131]

Lyu S, DeAndrade MP, Mueller S, Oksche A, Walters AS, Li Y (2019a) Hyperactivity, dopaminergic abnormalities, iron deficiency and anemia in an in vivo opioid receptors knockout mouse: Implications for the restless legs syndrome. Behav Brain Res 374:112123. [PubMed: 31376441]

Lyu S, Xing H, DeAndrade MP, Liu Y, Perez PD, Yokoi F, Febo M, Walters AS, Li Y (2019b) The role of BTBD9 in striatum and restless legs syndrome. eNeuro: 0277–19.2019.

Lyu S, Xing H, DeAndrade MP, Perez PD, Zhang K, Liu Y, Yokoi F, Febo M, Walters AS, Li Y (2019c) The role of BTBD9 in the cerebral cortex and the pathogenesis of restless legs syndrome. Experimental Neurology:113111. [PubMed: 31715135]

Marconi S, Scaglione C, Pizza F, Rizzo G, Plazzi G, Vetrugno R, La Manna G, Campieri C, Stefoni S, Montagna P, Martinelli P (2012) Group I nonreciprocal inhibition in restless legs syndrome secondary to chronic renal failure. Parkinsonism Relat Disord 18:362–366. [PubMed: 22197122]

Meiser J, Weindl D, Hiller K (2013) Complexity of dopamine metabolism. Cell Commun Signal 11:34. [PubMed: 23683503]

Meneely S, Dinkins M-L, Kassai M, Lyu S, Liu Y, Lin C-T, Brewer K, Li Y, Clemens S (2018) Differential dopamine D1 and D3 receptor modulation and expression in the spinal cord of two mouse models of Restless Legs Syndrome. Frontiers in Behavioral Neuroscience 12:199. [PubMed: 30233336]

Michaud M, Soucy JP, Chabli A, Lavigne G, Montplaisir J (2002) SPECT imaging of striatal pre- and postsynaptic dopaminergic status in restless legs syndrome with periodic leg movements in sleep. J Neurol 249:164–170. [PubMed: 11985381]

Ondo WG, He Y, Rajasekaran S, Le WD (2000) Clinical correlates of 6-hydroxydopamine injections into A11 dopaminergic neurons in rats: a possible model for restless legs syndrome. Mov Disord 15:154–158. [PubMed: 10634257]

Paladini CA, Robinson S, Morikawa H, Williams JT, Palmiter RD (2003) Dopamine controls the firing pattern of dopamine neurons via a network feedback mechanism. Proc Natl Acad Sci U S A 100:2866–2871. [PubMed: 12604788]

Qu S, Le W, Zhang X, Xie W, Zhang A, Ondo WG (2007) Locomotion is increased in a11-lesioned mice with iron deprivation: a possible animal model for restless legs syndrome. J Neuropathol Exp Neurol 66:383–388. [PubMed: 17483695]

Ringstad N, Horvitz HR (2008) FMRFamide neuropeptides and acetylcholine synergistically inhibit egg-laying by C. elegans. Nat Neurosci 11:1168–1176. [PubMed: 18806786]

Rooney KF, Sewell RD (1989) Evaluation of selective actions of dopamine D-1 and D-2 receptor agonists and antagonists on opioid antinociception. Eur J Pharmacol 168:329–336. [PubMed: 2573534]

Schafer WR (2005) Egg-laying In. WormBook: The C. elegans Research Community.

Schafer WR, Kenyon CJ (1995) A calcium-channel homologue required for adaptation to dopamine and serotonin in Caenorhabditis elegans. Nature 375:73–78. [PubMed: 7723846]

Schormair B et al. (2017) Identification of novel risk loci for restless legs syndrome in genome-wide association studies in individuals of European ancestry: a meta-analysis. Lancet Neurol 16:898–907. [PubMed: 29029846]

Spijker S (2011) Dissection of Rodent Brain Regions. Neuroproteomics 57:13–26.

Stefansson H et al. (2007) A genetic risk factor for periodic limb movements in sleep. The New England journal of medicine 357:639–647. [PubMed: 17634447]

Stogios PJ, Prive GG (2004) The BACK domain in BTB-kelch proteins. Trends Biochem Sci 29:634–637. [PubMed: 15544948]

Stogios PJ, Downs GS, Jauhal JJ, Nandra SK, Prive GG (2005) Sequence and structural analysis of BTB domain proteins. Genome Biol 6:R82. [PubMed: 16207353]

Thompson D, Martini L, Whistler JL (2010) Altered ratio of D1 and D2 dopamine receptors in mouse striatum is associated with behavioral sensitization to cocaine. PLoS One 5:e11038. [PubMed: 20543951]

Thompson ML, Chen P, Yan X, Kim H, Borom AR, Roberts NB, Caldwell KA, Caldwell GA (2014) TorsinA rescues ER-associated stress and locomotive defects in C. elegans models of ALS. Dis Model Mech 7:233–243. [PubMed: 24311730]

Tings T, Baier PC, Paulus W, Trenkwalder C (2003) Restless Legs Syndrome induced by impairment of sensory spinal pathways. J Neurol 250:499–500. [PubMed: 12760388]

Trenkwalder C, Paulus W, Walters AS (2005) The restless legs syndrome. Lancet neurology 4:465–475. [PubMed: 16033689]

Trenkwalder C, Allen R, Hogl B, Clemens S, Patton S, Schormair B, Winkelmann J (2018) Comorbidities, treatment, and pathophysiology in restless legs syndrome. Lancet Neurol 17:994–1005. [PubMed: 30244828]

Trent C, Tsuing N, Horvitz HR (1983) Egg-laying defective mutants of the nematode Caenorhabditis elegans. Genetics 104:619–647. [PubMed: 11813735]

Verma A, Kulkarni SK (1993) Modulatory role of D-1 and D-2 dopamine receptor subtypes in nociception in mice. J Psychopharmacol 7:270–275. [PubMed: 22290841]

Waggoner LE, Zhou GT, Schafer RW, Schafer WR (1998) Control of alternative behavioral states by serotonin in Caenorhabditis elegans. Neuron 21:203–214. [PubMed: 9697864]

Wall NR, De La Parra M, Callaway EM, Kreitzer AC (2013) Differential innervation of direct- and indirect-pathway striatal projection neurons. Neuron 79:347–360. [PubMed: 23810541]

Weinshenker D, Garriga G, Thomas JH (1995) Genetic and pharmacological analysis of neurotransmitters controlling egg laying in C. elegans. J Neurosci 15:6975–6985. [PubMed: 7472454]

Winkelmann J et al. (2007) Genome-wide association study of restless legs syndrome identifies common variants in three genomic regions. Nature genetics 39:1000–1006. [PubMed: 17637780]

Yokoi F, Dang MT, Liu J, Gandre JR, Kwon K, Yuen R, Li Y (2015) Decreased dopamine receptor 1 activity and impaired motor-skill transfer in Dyt1 DeltaGAG heterozygous knock-in mice. Behav Brain Res 279:202–210. [PubMed: 25451552]

Yokota T, Hirose K, Tanabe H, Tsukagoshi H (1991) Sleep-related periodic leg movements (nocturnal myoclonus) due to spinal cord lesion. J Neurol Sci 104:13–18. [PubMed: 1919596]

Zarrindast MR, Moghaddampour E (1989) Opposing influences of D-1 and D-2 dopamine receptors activation on morphine-induced antinociception. Arch Int Pharmacodyn Ther 300:37–50. [PubMed: 2619426]

Zhao H, Zhu W, Pan T, Xie W, Zhang A, Ondo WG, Le W (2007) Spinal cord dopamine receptor expression and function in mice with 6-OHDA lesion of the A11 nucleus and dietary iron deprivation. J Neurosci Res 85:1065–1076. [PubMed: 17342757]

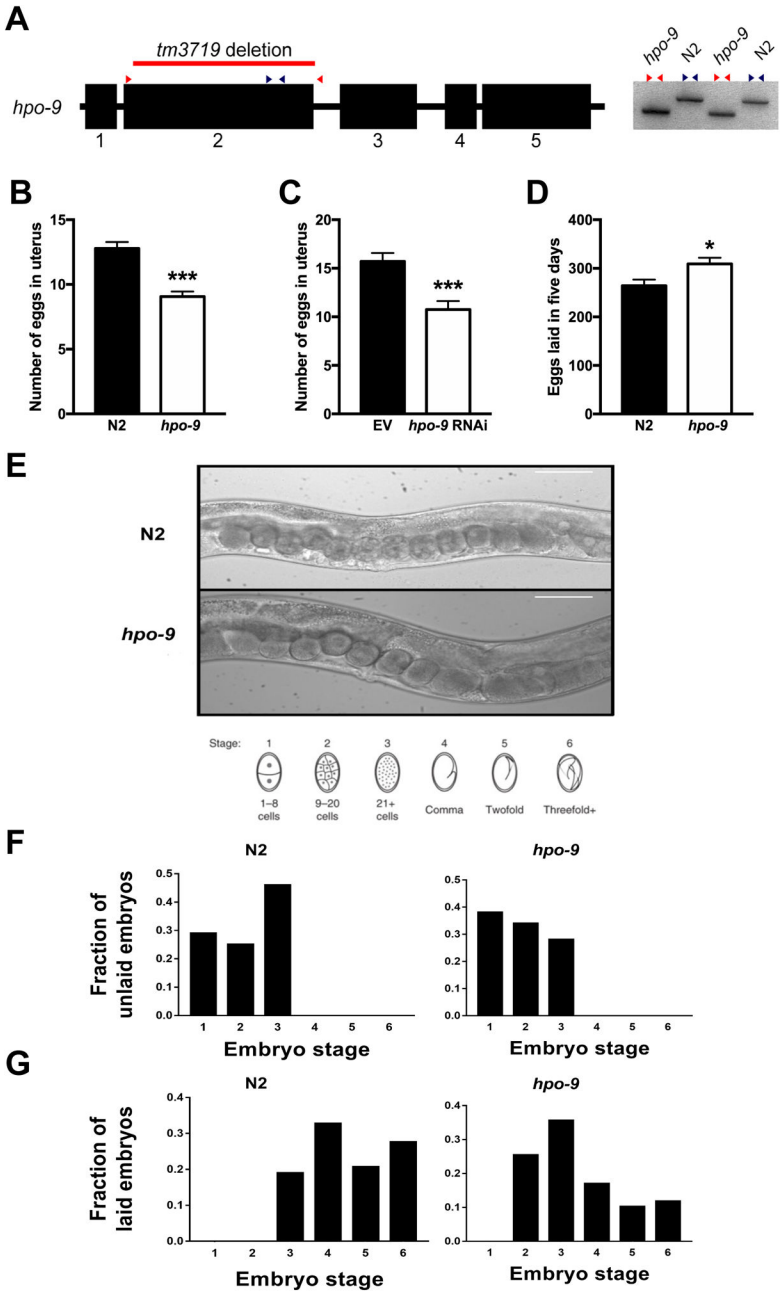

Figure 1.

Generation of *hpo-9(tm3719)* worm and egg laying behavior. (A) *hpo-9* gene structure and *tm3719* mutation. Black rectangular boxes denote coding exons. Redline above shows the genomic region deleted. The sites of the PCR primers are indicated by arrowheads, with black for N2 and red for *hpo-9(tm3719)* mutant. The PCR result is presented at right, confirming the successful deletion of the *hpo-9* allele. (B, C) Egg retention assay. (D) Egg-laying assay. *, $p < 0.05$; ***, $p < 0.005$. Bars represent the means plus SEs for 7–20 animals of each strain. (E) Representative pictures of N2 and *hpo-9(tm3719)* worms 22 hrs after the L4 stage. Scale bar represents 50 μm. (F, G) Embryo stages of unlaid and laid eggs.

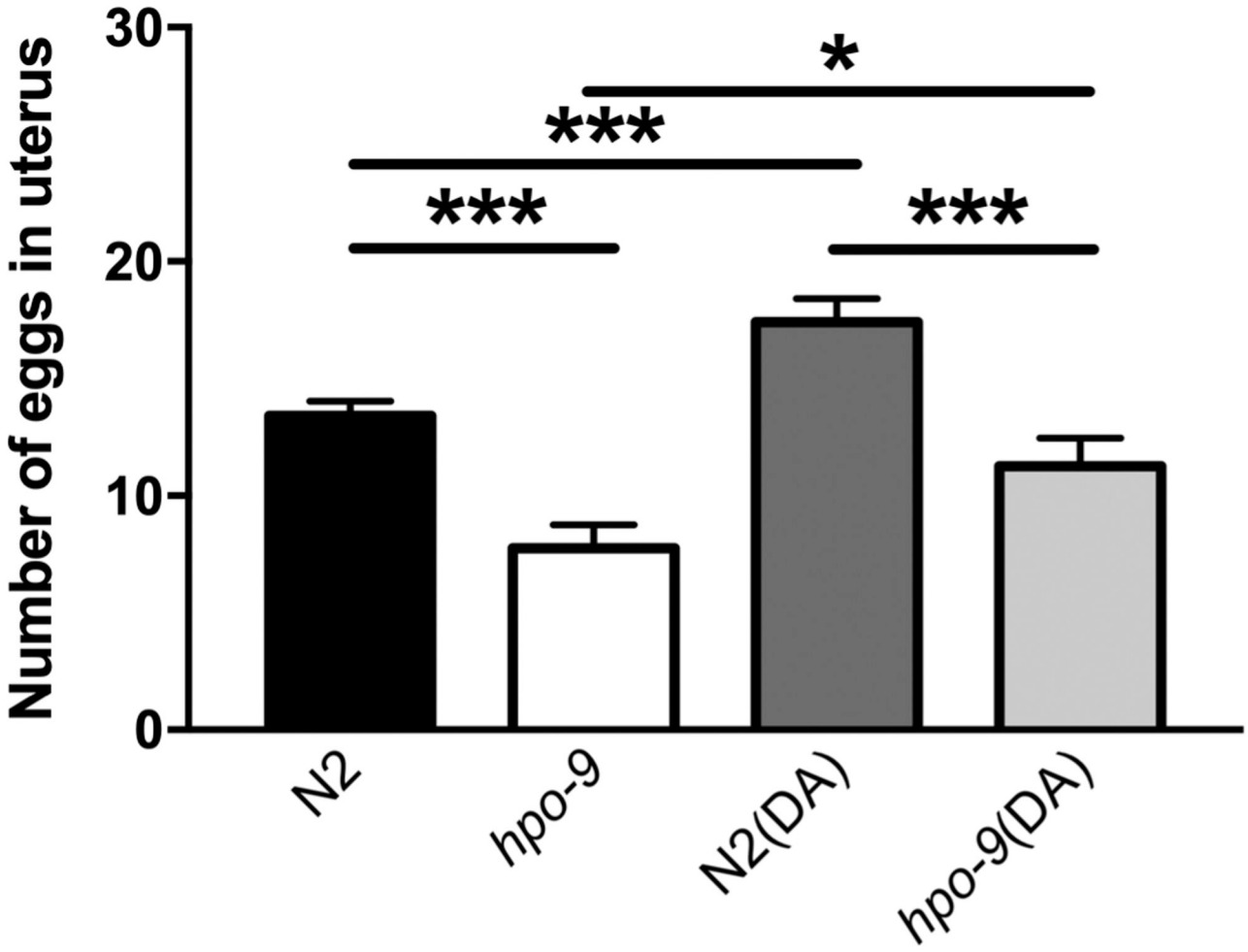

Figure 2.

Egg retention assay with or without the pretreatment of DA. The numbers of eggs retained were increased with DA treatment in both N2 and *hpo-9(tm3719)* strains. *hpo-9(tm3719)* had fewer eggs than N2 under either situation. Bars represent the means plus SEs for 12 animals for each strain. *, $p < 0.05$; ***, $p < 0.005$. *hpo-9*, *hpo-9(tm3719)* worms.

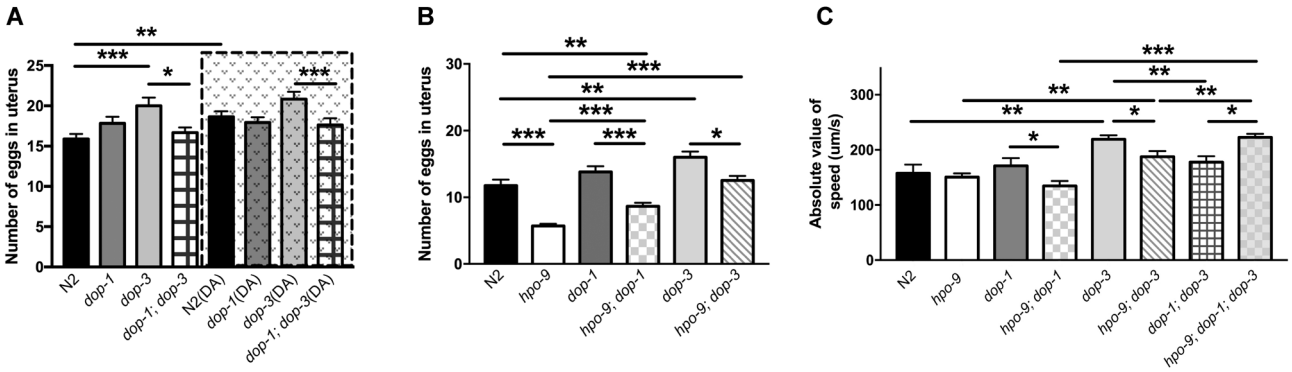

Figure 3.

Egg retention assay and WormLab recording showing relationship among *hpo-9*, *dop-1* and *dop-3*. Bars represent the means plus SEs for 10–20 animals of each strain. *, $p < 0.05$; **, $p < 0.01$; ***, $p < 0.005$. *hpo-9*, *hpo-9(tm3719)* worms. *dop-1*, *dop-1 (vs100)* worms. *dop-3*, *dop-3(vs106)* worms. *dop-1; dop-3*, *dop-1(vs100); dop-3(vs106)* worms. *hpo-9; dop-1*, *hpo-9(tm3719)*; *dop-1(vs100)* worms. *hpo-9; dop-3*, *hpo-9(tm3719)*; *dop-3(vs106)* worms. *hpo-9; dop-1; dop-3*, *hpo-9(tm3719)*; *dop-1(vs100); dop-3(vs106)* worms.

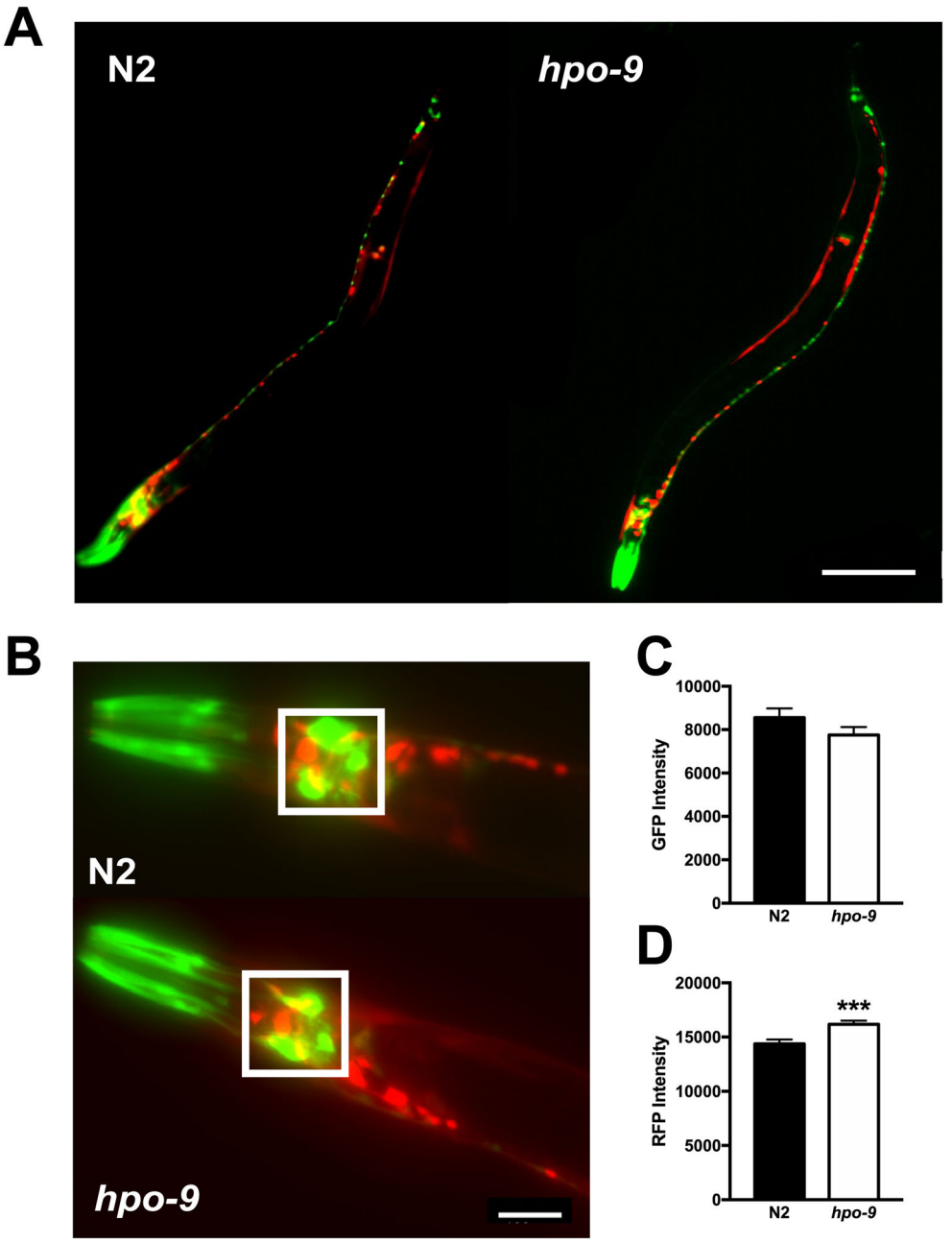

Figure 4.

Altered expression levels of DA receptors in the *hpo-9* strain. (A) Representative fluorescent micrographs of animals expressing the *dop-1*::*gfp*; *dop-3*::*rfp* alone (left panel) and with *hpo-9* knocked out (right panel). Scale bar represents 100 μm. (B) The image depicts the anterior region of *C. elegans*, and the boxed region indicates the head area where measurements of fluorescence were taken in all animals. Scale bar represents 25 μm. (C) Bar chart representing GFP intensity values (DOP-1) measured in the boxed region shown in B. (D) Bar chart representing RFP intensity values (DOP-3) measured in the boxed region shown in B. Bars represent the means plus SEs for 30 animals of each strain. ***, $p < 0.005$. *hpo-9*, *hpo-9(tm3719)* worms.

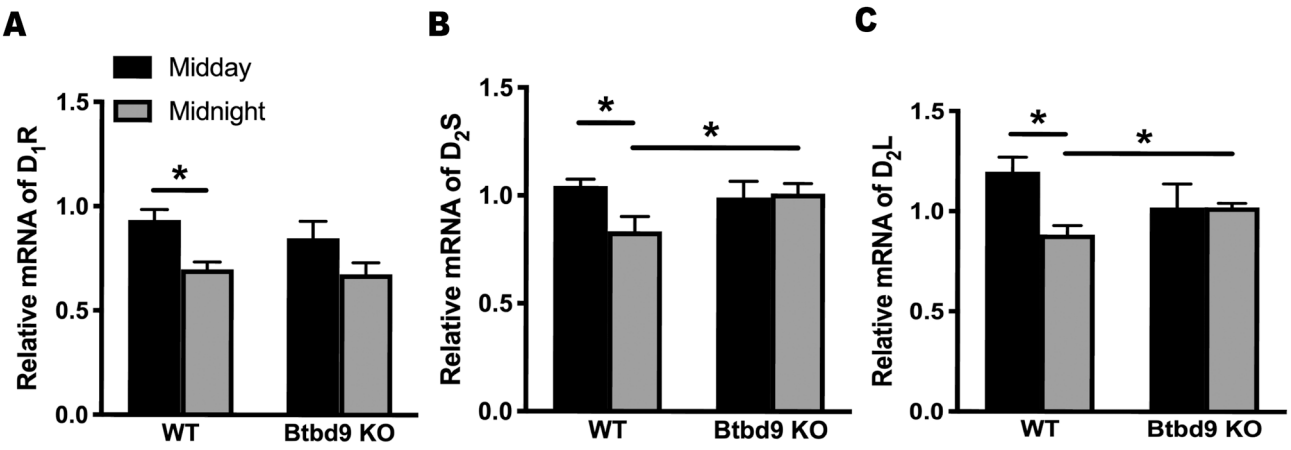

Figure 5.

Increased D2R mRNA levels during midnight (B, C) and an absence of circadian variations in the *Btbd9* KO mice (A-C). Bars represent the means plus SEs. Midday: WT, n=3, *Btbd9* KO, n=3; Midnight: WT, n=5, *Btbd9* KO, n=4. *, $p < 0.05$. KO, knockout.

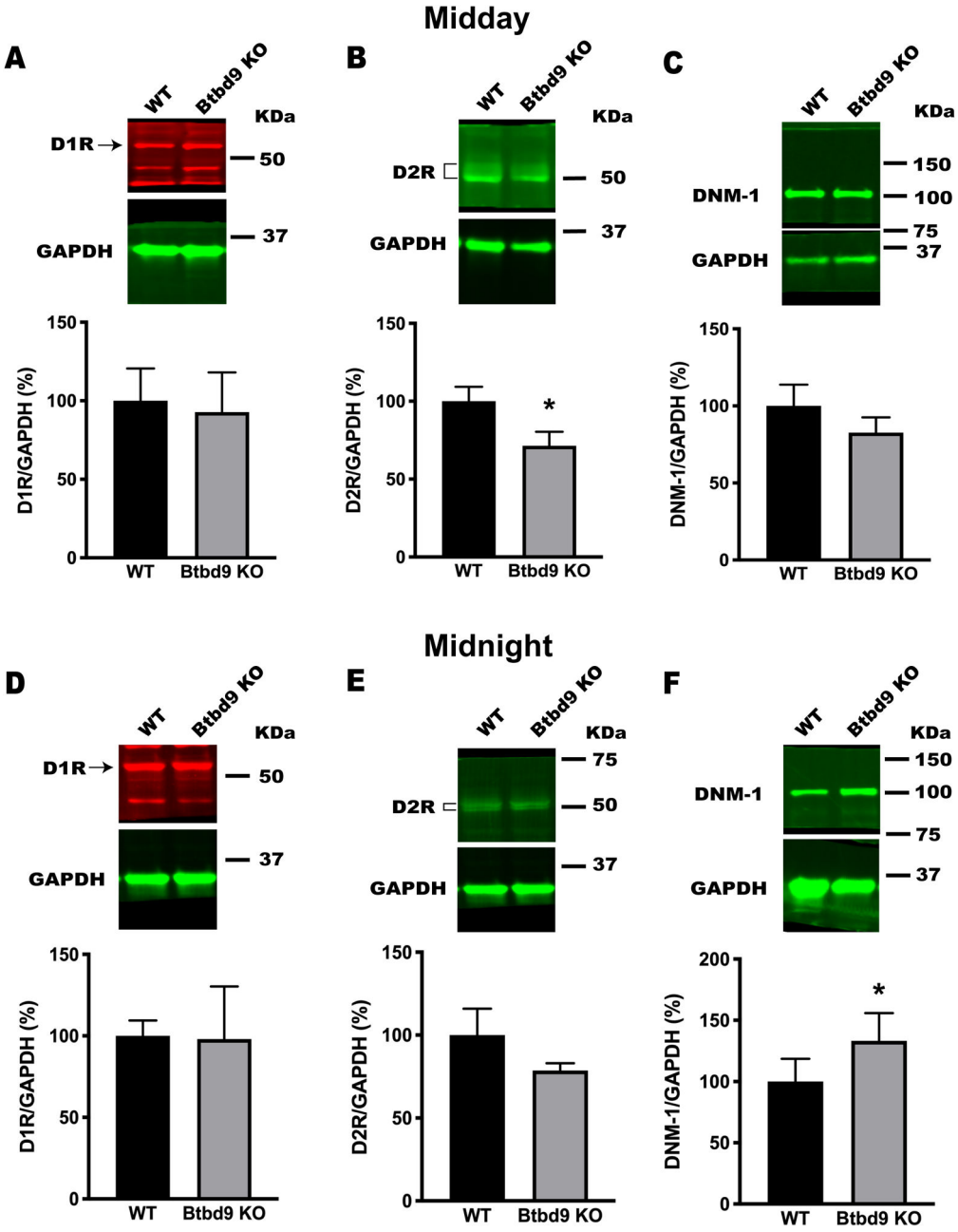

Figure 6.

Western blot analysis of D_1R, D_2R, and DNM-1 protein levels in the striata of *Btbd9* complete knockout and their WT littermates. (A) D_1R protein levels were not changed in *Btbd9* complete knockout mice compared with WT littermates at midday. (B) D_2R protein levels were significantly decreased in *Btbd9* complete knockout mice at the midday. (C) DNM-1 protein levels were not changed in *Btbd9* complete knockout mice compared with WT littermates at midday. (D) D_1R protein levels were not changed in *Btbd9* complete knockout mice compared with WT littermates at midnight. (E) D_2R protein levels were not significantly decreased in *Btbd9* complete knockout mice at midnight. (F) DNM-1 protein levels were significantly increased in *Btbd9* complete knockout mice at midnight. Target

protein levels were normalized to the GAPDH. Blots were cropped to show representative bands. Bars represent the means plus SEs (A-E) or means with 95% confident intervals (CIs, F). Midday: WT, n=6, *Btbd9* KO, n=7; midnight: WT, n=7, *Btbd9* KO, n=6. *, $p < 0.05$. KO, knockout.

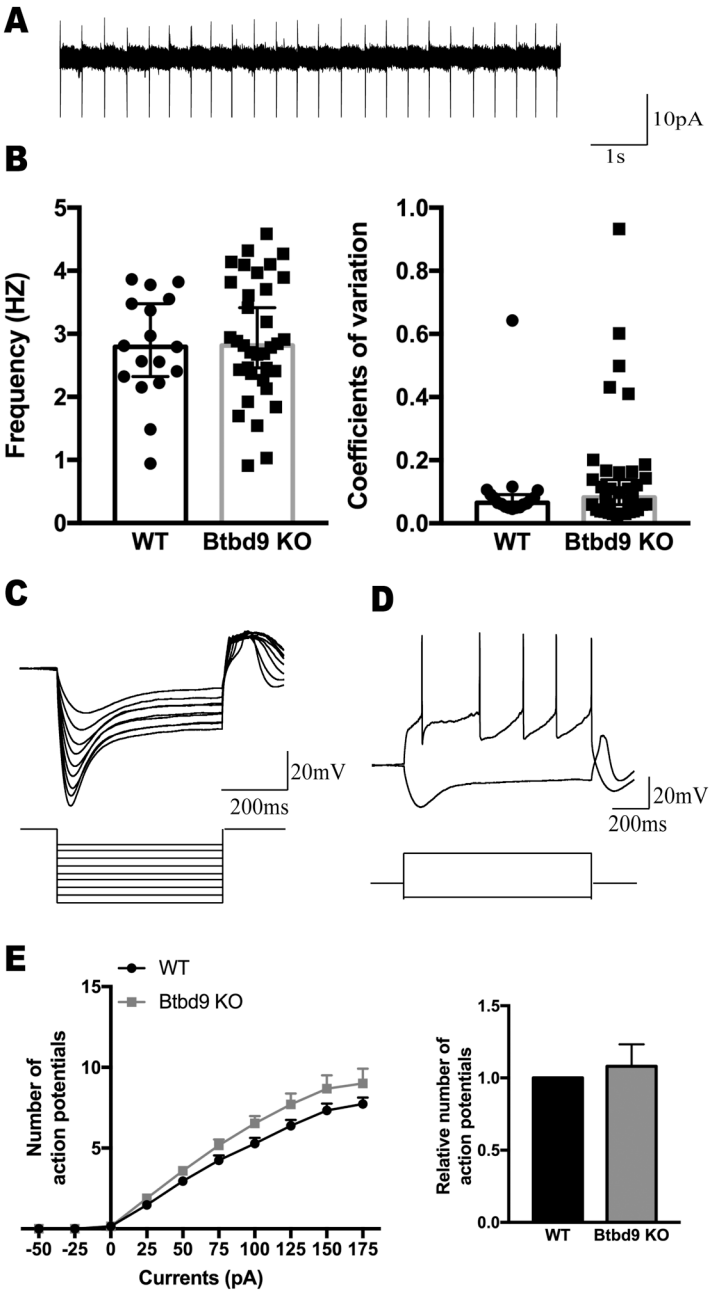

Figure 7.

In vitro recording of DA neurons (WT, n=17; *Btbd9* KO, n=35) in SN. (A) A representative spontaneous activity trace of a DA neuron. (B) Both spontaneous firing frequency and regularity were not significantly different between *Btbd9* KO and WT mice. (C) Identification of DA neurons in SN pars compacta from current-clamp recordings. DA neurons exhibit a prominent time-dependent sag in the voltage deflection in response to hyperpolarizing current injection. (D) A representative trace of DA neurons in response to current steps at 100pA (top), and -50 pA (bottom). (E) In response to the step current injection, DA neurons of *Btbd9* complete knockout mice fired a similar number of action potentials compared with the WT mice. Data in B and C were presented as median with 95%

CIs. Data in figure E were analyzed after log transformation. GEE model normalized the WT to 1 without the error bar (see Method). KO, knockout.

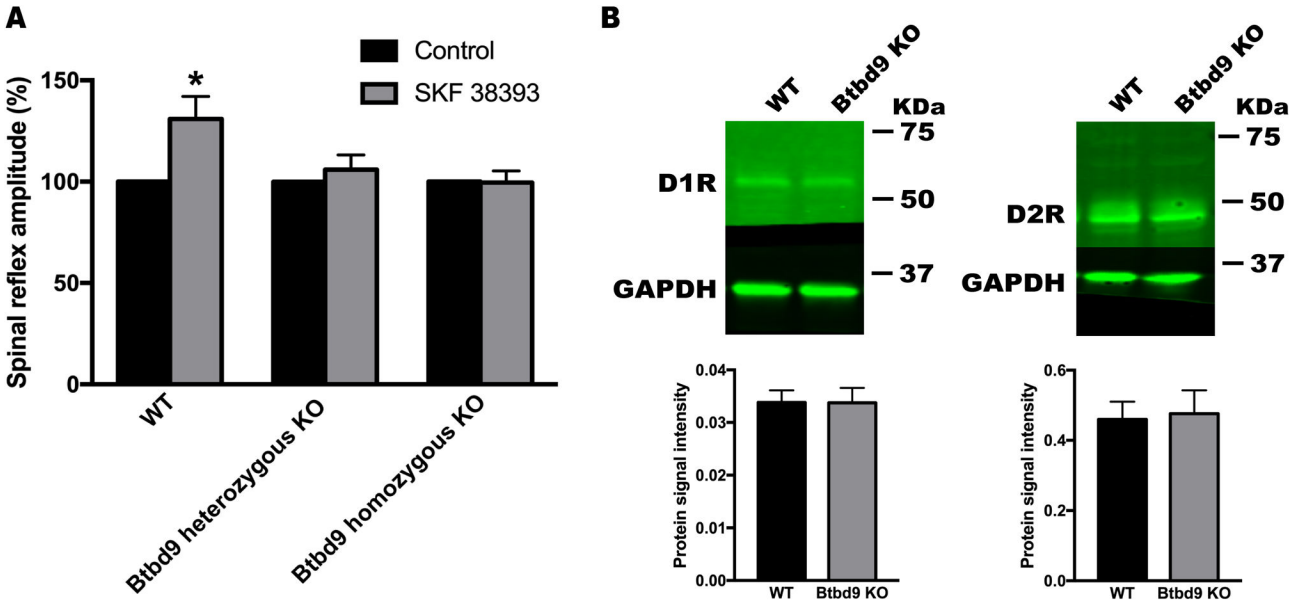

Figure 8.

The effects of a D_1R agonist, SKF 38393, on SRAs and Western blot analysis of D_1R and D_2R protein levels in the lumbar spinal cord. (A) SKF increased the SRAs in WT mice (n=8) but did not influence the SRAs in *Btbd9* heterozygous (n=6) and homozygous knockout mice (n=4). (B) *Btbd9* complete knockout mice (n=5) had the same level of D_1R and D_2R proteins in the lumbar spinal cord as WT mice (n=3). Target protein levels were normalized to the GAPDH. Blots were cropped to show representative bands. Bars represent the means plus SEs. *, $p < 0.05$. KO, knockout.

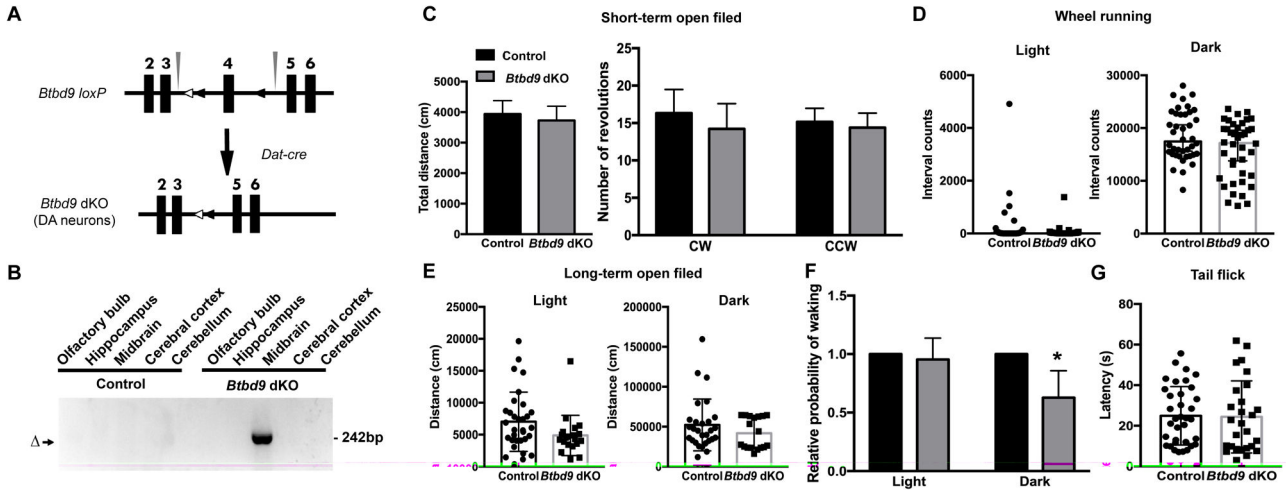

Figure 9.

Generation of *Btbd9* dKO mice and behavioral tests. (A) Schematic diagram of the generation of the *Btbd9* dKO mice. Filled boxes represent exons. Filled triangles indicate *loxP* sites. Open triangles indicate the *FRT* sites that were incorporated to remove the neo cassette. In *Btbd9* dKO mice, exon 4 is deleted in DA neurons because *cre* is expressed specifically in DA neurons, and the recombination occurs in the cells. The gray arrows indicate the sites of the PCR primers used to detect the knockout. (B) Tissue-specific deletion of *Btbd9* exon 4 in *Btbd9* dKO mice was confirmed by PCR using DNA isolated from each brain region. The deletion was detected only in the midbrain (includes SN) of *Btbd9* dKO mouse as predicted (Δ). (C) 30-min open field test (*Btbd9* dKO, n=7; controls, n=8). (D) Wheel running test (*Btbd9* dKO, n=10, controls, n=10). (E-F) Continuous open filed test (*Btbd9* dKO, n=5; controls, n=8). (G) Tail-flick experiment (*Btbd9* dKO, n=9; controls n=12). The data in figure D-G were analyzed after log transformation. GEE model normalized the control group to 1 without the error bar (see Method). Bars represent means plus standard errors (SEs). The data in Figures D, E and G were presented as median with 95% CIs. *, $p < 0.05$.

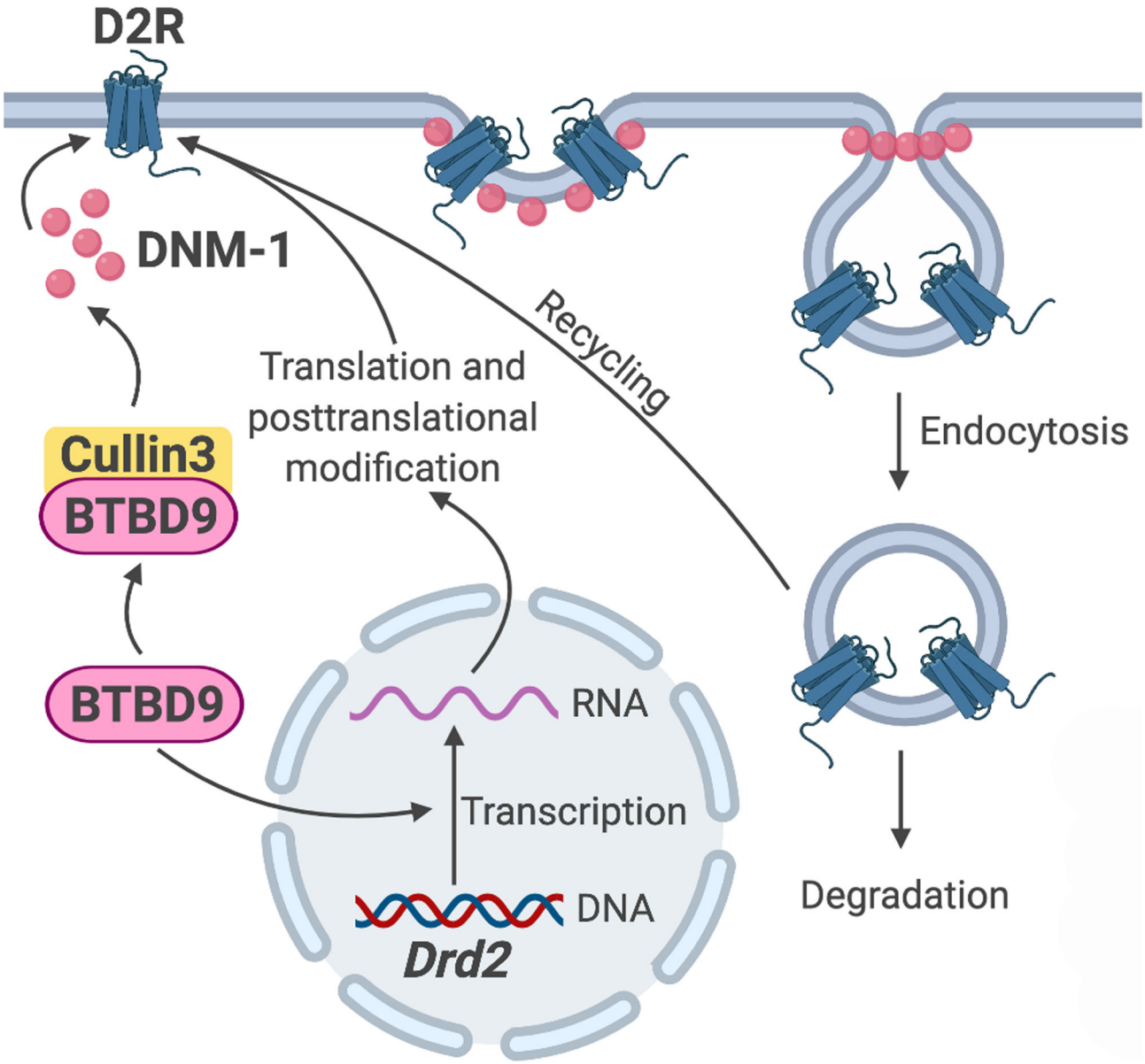

Figure 10.

Model of regulation of D2R by BTBD9. BTBD9 acts as an adaptor for E3 ubiquitin ligase, which is necessary for the degradation of DNM-1. DNM-1 participates in the endocytosis of D2R. Therefore, BTBD9 deficiency leads to increased DNM-1 level and decreased D2R level. BTBD9 may also regulate the transcription of D2R.